nature aging

Article

https://doi.org/10.1038/s43587-024-00798-7

Niche-derived Semaphorin 4A safeguards functional identity of myeloid-biased hematopoietic stem cells

Received: 8 August 2024

Accepted: 17 December 2024

Published online: 29 January 2025

Check for updates

Dorsa Toghani[1,16], Sanika Gupte[1,16], Sharon Zeng[1], Elmir Mahammadov[2], Edie I. Crosse[1], Negar Seyedhassantehrani[3], Christian Burns[3], David Gravano[3], Stefan Radtke[1], Hans-Peter Kiem[1], Sonia Rodriguez[4], Nadia Carlesso[4], Amogh Pradeep[1], Alexis Georgiades[1], Fabienne Lucas[1], Nicola K. Wilson[5], Sarah J. Kinston[5], Berthold Göttgens[5], Le Zong[6], Isabel Beerman[6], Bongsoo Park[6], Derek H. Janssens[7], Daniel Jones[1], Ali Toghani[1], Claus Nerlov[8], Eric M. Pietras[9], Marion Mesnieres[10], Christa Maes[10], Atsushi Kumanogoh[11], Thomas Worzfeld[12], Jin-Gyu Cheong[13,14], Steven Z. Josefowicz[13,14], Peter Kharchenko[15], David T. Scadden[15], Antonio Scialdone[2], Joel A. Spencer[3] & Lev Silberstein[1]

Somatic stem cell pools comprise diverse, highly specialized subsets whose individual contribution is critical for the overall regenerative function. In the bone marrow, myeloid-biased hematopoietic stem cells (myHSCs) are indispensable for replenishment of myeloid cells and platelets during inflammatory response but, at the same time, become irreversibly damaged during inflammation and aging. Here we identify an extrinsic factor, Semaphorin 4A (Sema4A), which non-cell-autonomously confers myHSC resilience to inflammatory stress. We show that, in the absence of Sema4A, myHSC inflammatory hyper-responsiveness in young mice drives excessive myHSC expansion, myeloid bias and profound loss of regenerative function with age. Mechanistically, Sema4A is mainly produced by neutrophils, signals via a cell surface receptor, Plexin D1, and safeguards the myHSC epigenetic state. Our study shows that, by selectively protecting a distinct stem cell subset, an extrinsic factor preserves functional diversity of somatic stem cell pool throughout organismal lifespan.

Cellular diversity is a fundamental feature of complex organisms because the presence of specialized cell types is beneficial for adaptability to environmental challenge and organismal survival[1]. Until recently, cellular diversity was considered a sole property of terminally differentiated cells, but recent studies have shown that, in multiple tissues, the most primitive cells—somatic stem cells—are also functionally diverse[1–5]. However, little is known about the signals that maintain unique functional identity of distinct stem cell subsets.

In mouse and human bone marrow, myeloid-biased hematopoietic stem cells (myHSCs) are a critical HSC subset that is specifically tasked with replenishment of mature myeloid cells and platelets during inflammatory response and likely serve as a long-lasting reservoir of inflammatory memory[6–16]. Because inflammation causes irreversible loss of HSC function[17], myHSCs must possess specific mechanisms that make them resilient to inflammatory stress. Failure of such mechanisms is exemplified by aging, which is characterized by excessive myHSC

A full list of affiliations appears at the end of the paper. e-mail: lsilbers@fredhutch.org

expansion and myeloid bias, leading to compromised immune function and increased risk of myeloid malignancy[18,19]. However, how myHSCs withstand inflammatory stress and resist premature loss of function with age is not known.

In the present study, we found that an extrinsic factor, Semaphorin 4A (Sema4A)[20–22], attenuates the inflammatory response of myHSCs and preserves their stemness and longevity. Sema4A acts in a non-cell-autonomous manner via binding to a cell surface receptor, Plexin D1 (PlxnD1)[23], and originates predominantly from mature neutrophils. Strikingly, the loss of Sema4A causes loss of myHSC self-renewal and myeloid lineage potential but is largely inconsequential for lymphoid-biased hematopoietic stem cells (lyHSCs). Thus, by maintaining functional identity of myHSCs, Sema4A safeguards the overall diversity of the HSC pool.

Results

Sema4A deletion leads to premature hematopoietic aging

We previously designed an in vivo platform for unbiased identification of HSC niche factors by comparing single-cell transcriptional signatures of stromal cells located in close proximity to transplanted HSCs and those further away, and we discovered several extrinsic regulators of HSC self-renewal[24,25]. Among the candidate molecules not yet characterized was Sema4A—an established regulator of neurogenesis, angiogenesis and immune response[23,26,27] with no known function in hematopoiesis.

While investigating the hematopoietic phenotype of Sema4A knockout (Sema4AKO) mice, we unexpectedly noticed that these animals developed progressive neutrophilia and thrombocytosis and anemia as they become fully aged (74–80 weeks old). (Fig. 1a–c). Histological examination of the bone marrow of these animals revealed a relative reduction of erythroid cells due to an expansion of myelopoieisis (myeloid hyperplasia), leading to an increased myeloid-to-erythroid (M:E) ratio (Fig. 1e,f). Myeloid hyperplasia also manifested as focal crowding of hematopoietic elements into the sub-epiphyseal fat space (Fig. 1d and Extended Data Fig. 1a), similar to the bone marrow findings in patients with myeloproliferative disorders[28]. These features represent hallmarks of hematopoietic aging[29] but were exaggerated in aged Sema4AKO mice, suggesting that the absence of Sema4A resulted in premature aging-like phenotype. Accordingly, aged Sema4AKO mice displayed significantly increased absolute numbers of HSCs and myeloid and megakaryocyte progenitors but decreased erythroid progenitors as well as expansion of mature myeloid cells but contraction of the B cell compartment (Fig. 1g–j). These changes were due to a difference in frequencies of these cellular subsets between aged wild-type (WT) and Sema4AKO mice, because the bone marrow cellularity was similar (Extended Data Fig. 1b).

To understand the molecular basis for the enhanced myelopoiesis in aged Sema4AKO mice, we performed bulk RNA sequencing (RNA-seq) analysis of phenotypic HSCs ($Lin^-Kit^+Sca^+CD48^-Flk2^-CD150^+$). Interestingly, aged Sema4AKO HSC transcriptome was significantly enriched for a transcriptional signature associated with myeloid differentiation[30], suggesting that enhanced myelopoiesis originates at the HSC level (Fig. 1k). This finding could be explained by either enhanced myeloid differentiation of the entire aged Sema4AKO HSC compartment or a compositional change, such as a higher relative proportion of myHSCs within aged Sema4AKO HSC pool[11]. Critically, quantification of myHSCs (defined as $Lin^-Kit^+Sca^+CD48^-Flk2^-CD150^{high}$; Extended Data Fig. 1c,d) revealed that they were markedly increased in aged Sema4AKO mice, whereas the number of lyHSCs ($Lin^-Kit^+Sca^+CD48^-Flk2^-CD150^{low}$) was similar between the groups (Fig. 1l,m and Extended Data Fig. 1e–g; see Supplementary Note 1 for validation of $CD150^{high}$ as a marker for aged Sema4AKO myHSCs). Thus, exaggerated and selective myHSC expansion likely accounts for myeloid bias and premature aging-like hematopoietic phenotype in Sema4AKO mice.

Aged Sema4AKO myHSCs selectively lose regenerative function

We next asked how the loss of Sema4A during aging impacts myHSC stemness, using competitive transplantation experiments. As a quality control for myHSC/lyHSC isolation, we calculated myeloid/lymphoid ratio in the recipients of WT myHSCs/lyHSCs and found that it was significantly higher in the former, as expected (Extended Data Fig. 2a,b). Strikingly, transplantation of equal numbers of aged WT/Sema4AKO myHSCs/lyHSCs into WT recipients revealed that, whereas aged Sema4AKO lyHSCs retained their competitive fitness, it was almost completely lost in aged Sema4AKO myHSCs, which failed to reconstitute in peripheral blood and the bone marrow (Fig. 2a–h and Extended Data Fig. 2c). Collectively, these data are consistent with selective and profound loss of regenerative capacity of aged Sema4AKO myHSCs, although a homing defect—a prominent feature of physiological aging[31]—may have also contributed to their engraftment failure.

Aiming to understand the molecular underpinnings of this phenotype, we performed single-cell RNA-seq analysis of myHSCs and lyHSCs from aged WT and Sema4AKO mice. Transcriptome-wide comparison revealed that, consistent with the myHSC-selective effect of Sema4A, aged myHSCs from WT and Sema4AKO mice formed distinct, minimally overlapping clusters, whereas the transcriptomes of aged WT and Sema4AKO lyHSCs were virtually indistinguishable (Fig. 2i,j and Extended Data Fig. 2d). Among differentially expressed genes (DEGs), aged Sema4AKO myHSCs displayed higher expression of AP-1 family transcription factors (*Jun*, *JunD*, *Fos* and *FosB*), which are known to be associated with inflammatory response and myeloid/megakaryocytic differentiation[32–37]. In contrast, several genes known to restrict HSC activation and inhibit differentiation (*Relb*, *Stat1*, *CD74* and *Irgm1*)[38–41] were downregulated (Extended Data Fig. 2e). Overall, these data suggest that in situ expanded aged Sema4AKO myHSCs are hypersensitive to inflammatory stress and primed for myeloid differentiation, which may explain their dramatically reduced regenerative capacity.

To further explore these findings, we performed diffusion pseudotime (DPT) analysis[42] (see Supplementary Note 2 for details), which quantifies the differentiation state of each cell going from naive (corresponding to HSCs) to less primitive (multipotent progenitors (MPPs)) state. In agreement with the published data[42], we observed that the DPT values for WT aged myHSCs were significantly lower than for WT aged lyHSCs, suggesting that myHSCs are positioned at the top of the HSC hierarchy (Extended Data Fig. 2f). Applying DPT analysis to the transcriptomes of WT and Sema4AKO aged myHSCs revealed that the DPT values for the latter were significantly higher and closer to that of WT lyHSCs, suggesting that the absence of Sema4A leads to myHSC shift to a more differentiated cellular state (Fig. 2k). In contrast, no difference in DPT values was observed between WT and Sema4AKO aged lyHSCs (Fig. 2l).

Given that the pro-inflammatory signature and accelerated differentiation—the hallmarks of HSC aging[43]—are more prominently displayed in the transcriptome of aged Sema4AKO myHSCs, we wondered whether these cells would be molecularly 'more aged' overall. We, therefore, projected a published 'aging signature'[44] onto the 'pseudo-bulk' single-cell RNA-seq signature of myHSCs from aged WT/Sema4AKO mice. As shown in Fig. 2m,n, both upregulated and downregulated transcripts in the 'aging signature' displayed significant enrichment for their respective counterparts in the aged Sema4AKO myHSC signature ($P < 0.01$, false discovery rate (FDR) < 0.01 in both directions), consistent with premature aging of Sema4AKO myHSCs.

Taken together, these data provide functional and molecular evidence that, during aging, Sema4A is required for myHSC resilience to inflammatory stress, prevention of differentiation and maintenance of stemness; however, Sema4A is largely dispensable for lyHSCs in this physiological context.

https://doi.org/10.1038/s43587-024-00798-7

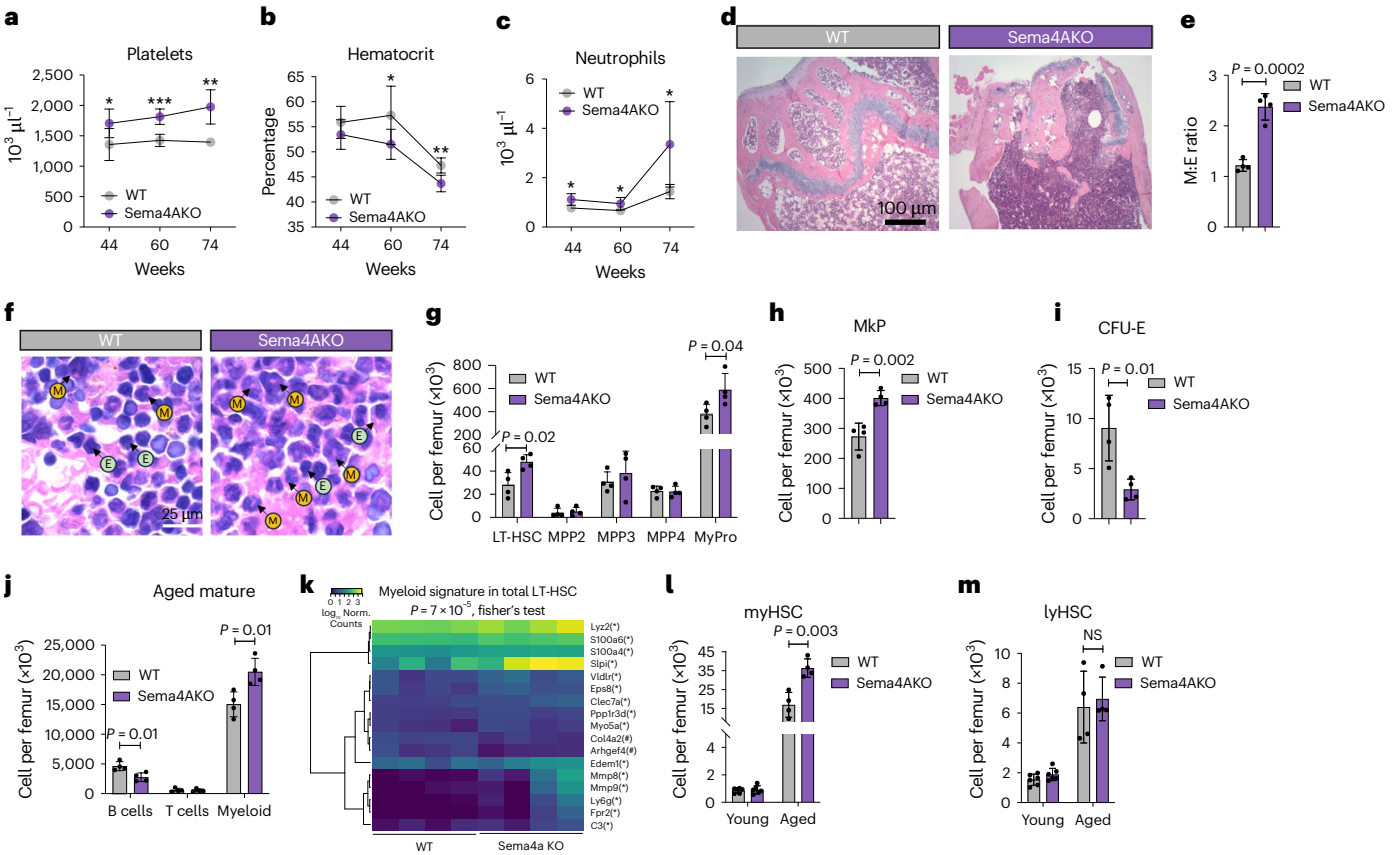

Fig. 1 | The absence of Sema4A leads to excessive myeloid expansion and premature hematopoietic aging-like phenotype. a–**c**, Platelet count (44 weeks, $P = 0.04$; 60 weeks, $P = 1.8 \times 10^{-5}$; 74 weeks, $P = 0.002$) (**a**), hematocrit level (60 weeks, $P = 0.03$; 74 weeks, $P = 0.002$) (**b**) and neutrophil count (44 weeks, $P = 0.02$; 60 weeks, $P = 0.02$; 74 weeks, $P = 0.02$) (**c**) in the peripheral blood of aged WT/Sema4AKO mice ($n = 5$ mice per group). **d**, Representative images of sub-epiphyseal area of H&E-stained femurs from aged WT/Sema4AKO mice ($n = 4$ mice per group). **e**, M:E ratio in the bone marrow of aged WT/Sema4AKO mice ($n = 4$ mice per group). **f**, Representative images of H&E staining of femurs from aged WT/Sema4AKO mice. Arrows with letters M and E indicate myeloid and erythroid cells, respectively ($n = 4$ mice per group). **g**–**j**, Absolute number of hematopoietic stem and progenitor subsets (**g**), megakaryocyte progenitors (MkPs) (**h**), erythroid progenitors (colony-forming unit–erythroid (CFU-E)) (**i**) and mature cells (**j**) in the bone marrow of aged WT/Sema4AKO mice ($n = 4$ mice per group). MyPro, myeloid progenitor. **k**, Projection of previously published myeloid signature onto the RNA-seq profiles of HSCs from aged WT/Sema4A mice ($n = 4$ animals per group). **l**,**m**, Absolute numbers of myHSCs (**l**) and lyHSCs (**m**) in the bone marrow of aged WT/Sema4AKO mice ($n = 5$ mice per group). *P* values are shown. For the peripheral blood counts, $^*P < 0.05$, $^{**}P < 0.01$, $^{***}P < 0.001$, NS, not significant. Statistical significance was assessed by two-tailed *t*-test. Mean ± s.e.m. values are shown.

Young Sema4AKO myHSCs are hyperactivated at the steady state

Having established that Sema4A is a critical hematopoietic regulator during aging, we wondered if hematopoiesis is already disrupted in young Sema4AKO mice. Indeed, we discovered that these animals also had neutrophilia and thrombocytosis, albeit considerably less prominent as in their aged counterparts (Fig. 3a); myeloid/platelet-biased multipotent progenitor MPP2 and mature myeloid cells were also increased, although selective myHSC expansion—the key feature of aged Sema4AKO phenotype—was not detectable (Fig. 3b–d).

Nevertheless, RNA-seq analysis showed that the absence of Sema4A induced evident transcriptional changes that were largely restricted to myHSCs. In particular, we found 154 DEGs between WT and Sema4AKO myHSCs but only 20 DEGs between WT and Sema4AKO lyHSCs, none of which was previously implicated in regulation of HSC function (Fig. 3e,f). Notably, Sema4AKO myHSC signature displayed increased expression of genes that promote HSC proliferation and loss of stemness (*Mki67*, *H2AX*, *CCNA2* and *Cdk6*), whereas expression of *Mpl* and *Irgm1*, which are involved in maintenance of stem cell state, was reduced[45–49]. In addition, gene set enrichment analysis (GSEA) revealed upregulation of several pathways involved in cellular proliferation ('E2F targets' and 'MYC targets') and metabolic activation ('Oxidative phosphorylation' and 'mTORC1 signaling') (Fig. 3g).

Collectively, the results of phenotypic and transcriptional analysis indicate that the absence of Sema4A leads to enhanced proliferative and metabolic activation of myHSCs (but not lyHSCs) at the steady state. In keeping with these data, cell cycle analysis and 5-bromo-2′-deoxyuridine (BrdU) incorporation studies revealed that Sema4AKO myHSC proliferation was increased, whereas Sema4AKO lyHSC proliferation was less uniformly affected and not statistically different between the groups (Extended Data Fig. 3a–d).

Young Sema4AKO myHSCs lose myeloid bias

Next, we investigated the impact of the above phenotypic and molecular abnormalities on young Sema4AKO myHSC function using competitive transplantation. We first confirmed that, similar to aged WT myHSCs, young WT myHSCs also produced a predominantly myeloid-biased graft, as evidenced by a higher myeloid/lymphoid ratio compared to young WT lyHSCs (Extended Data Fig. 3e). Transplantation of young Sema4AKO myHSCs revealed that, although they generated a higher level of donor chimerism, the frequency of long-term HSCs (LT-HSCs) in the post-transplant bone marrow was lower, indicating the loss of self-renewal. In contrast, the absence of Sema4A had little effect on

https://doi.org/10.1038/s43587-024-00798-7

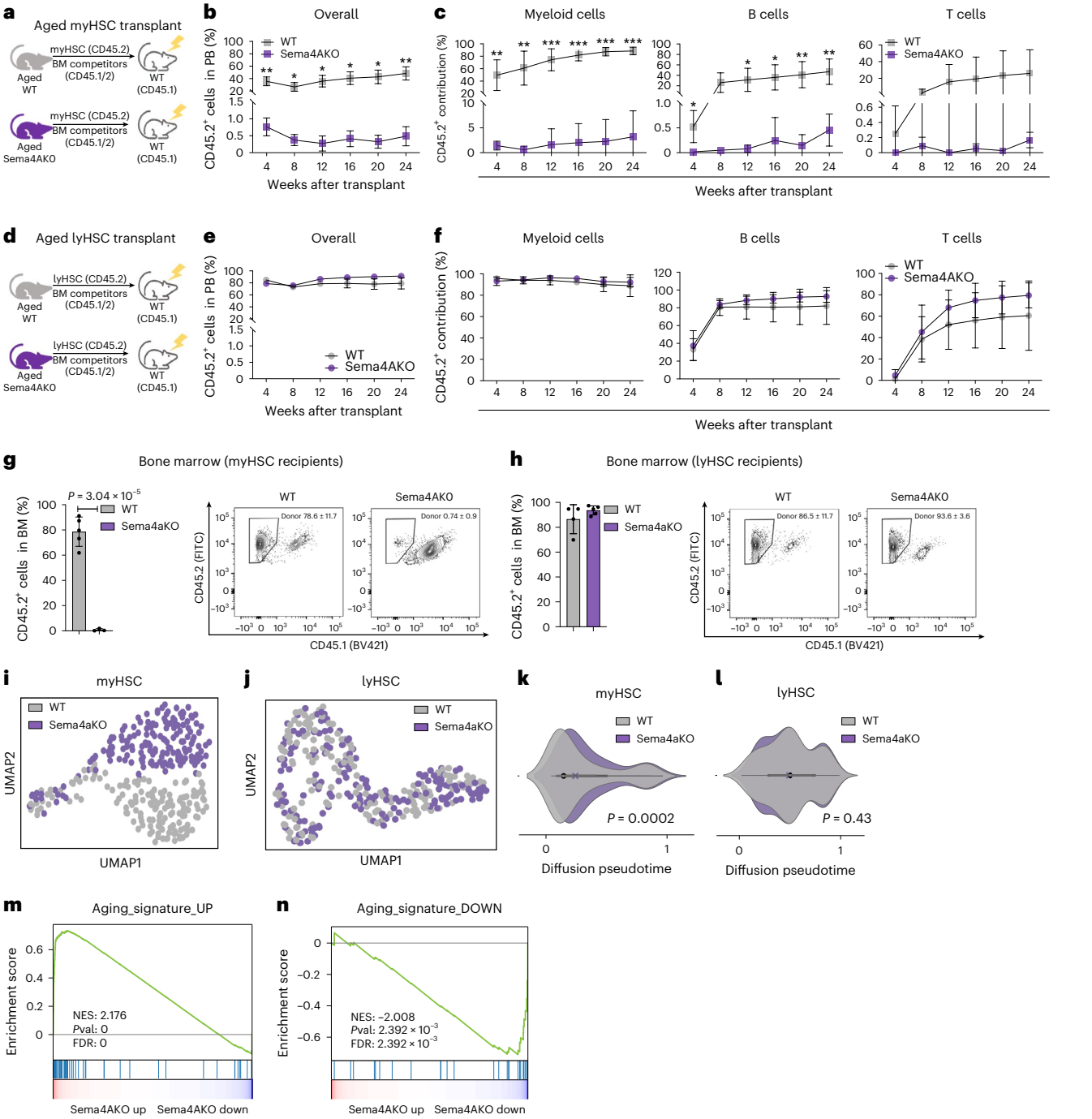

Fig. 2 | The absence of Sema4A leads to functional attrition of myHSCs during aging. a–**c**, Experimental schema (**a**), overall percentage of donor-derived peripheral blood cells (4 weeks, $P = 0.003$; 8 weeks, $P = 0.01$; 12 weeks, $P = 0.01$; 16 weeks, $P = 0.01$; 20 weeks, $P = 0.01$; 24 weeks, $P = 0.006$) (**b**) and lineage contribution by donor-derived cells (myeloid cells: 4 weeks, $P = 0.006$; 8 weeks, $P = 0.003$; 12 weeks, $P = 8.9 \times 10^{-5}$; 16 weeks, $P = 8.8 \times 10^{-7}$; 20 weeks, $P = 1.1 \times 10^{-7}$; 24 weeks, $P = 1.0 \times 10^{-7}$; B cells: 4 weeks, $P = 0.02$; 12 weeks, $P = 0.03$; 16 weeks, $P = 0.02$; 20 weeks, $P = 0.01$; 24 weeks, $P = 0.007$) (**c**) after competitive transplantation of WT/Sema4AKO myHSCs (CD45.2) into WT recipients (CD45.1) ($n = 5$ animals per group). **d**–**f**, Experimental schema (**d**), overall percentage of donor-derived peripheral blood cells (**e**) and lineage contribution by donor-derived cells (**f**) after competitive transplantation of WT/Sema4AKO lyHSCs (CD45.2) into WT recipients (CD45.1) ($n = 5$ animals per group). **g**,**h**, Overall percentage of donor-derived cells in the bone marrow after competitive transplantation of WT/Sema4AKO myHSCs (CD45.2) (**g**) and WT/Sema4AKO lyHSCs (CD45.2) (**h**) into WT recipients (CD45.1); quantification and representative plot for the overall bone marrow chimerism are shown ($n = 5$ animals per group). **i**,**j**, UMAP representation of 162 myHSCs (**i**) and 165 lyHSCs (**j**) from aged WT and Sema4AKO mice ($n = 2$ mice per genotype). **k**,**l**, Distribution of DPT values of myHSCs ($n = 322$ cells across two biological replicates and four technical replicates) (**k**) and lyHSCs ($n = 320$ cells across two biological replicates and four technical replicates) (**l**) from aged WT and Sema4AKO mice. In the inner box plots of the violin plots, the white point shows the median value; box limits indicate upper and lower quartiles; and whiskers extend to minimum and maximum values. **m**,**n**, Enrichment of upregulated and downregulated genes in the aged Sema4AKO myHSC signature for the upregulated (**m**) and downregulated (**n**) genes in the HSC 'aging signature'[44] as assessed by GSEA. *P* values are shown and were determined using using random permutation test. For the transplant experiments, $^*P < 0.05$ and $^{**}P < 0.01$. Statistical significance was assessed by two-tailed *t*-test, except for the DPT analysis where two-tailed Wilcoxon rank-sum test was used. Mean ± s.e.m. values are shown. BM, bone marrow; NES, normalized enrichment score; PB, peripheral blood; Pval, *P* value.

reconstitution capacity and self-renewal of lyHSCs (Fig. 3n). Overall, these data demonstrate that, in young animals, Sema4A predominantly regulates myHSC function.

Previous studies reported that, as we also observed, WT myHSCs normally produce a lower level of donor chimerism compared to lyHSCs, which is associated with their predominantly myeloid differentiation and suppression of the lymphoid potential[13]. Given that the level Sema4AKO myHSC-generated chimerism was abnormally high, we wondered if it would be associated with the loss of the myeloid potential and enhanced lymphoid-biased differentiation. Indeed, the myeloid/lymphoid ratio of Sema4AKO myHSC-derived progeny was significantly lower than that of their WT counterparts, consistent with the lymphoid-skewed differentiation. Notably, by post-transplant week 24, the myeloid/lymphoid ratio in the Sema4AKO myHSC cohort became almost identical to that of the WT lyHSC cohort (~0.1) (Fig. 3o; compare to Extended Data Fig. 3e), indicating that Sema4AKO myHSCs were no longer 'myeloid biased'.

Post-transplant bone marrow findings further reinforced this conclusion. As expected, in the WT myHSC recipients, the frequency of lymphoid-biased Flk2$^{med/high}$ multipotent progenitor MPP4 (refs. 50,51) and their level of Flk2 expression were lower compared to the WT lyHSC cohort, consistent with intact myeloid potential (Extended Data Fig. 3f,g). In contrast, in the Sema4AKO myHSC recipients, both MPP4 frequency and Flk2 expression level were increased and similar to those observed in the WT lyHSC cohort, consistent with lymphoid skewing. Taken together, the results of post-transplant blood and bone marrow analysis show that, in the absence of Sema4A, young myHSCs acquire increased lymphoid differentiation potential and lose myeloid bias—the key feature of their functional identity.

Sema4AKO myHSCs are hypersensitive to acute inflammation

Given that myHSC-driven inflammatory myelopoiesis is critical for host defense against bacterial pathogens and that myHSCs express higher levels of TLR4 (ref. 52), we next tested the impact of Sema4A on myHSC response to TLR4 agonist lipopolysaccharide (LPS)[53]. We first employed an acute LPS treatment model (a single LPS dose (4 mg kg^{-1})) (Fig. 4a). As expected, WT myHSCs (as well as myeloid-biased multipotent progenitors MPP2 and MPP3) displayed the greatest expansion at 72 h after LPS injection, with myHSCs comprising approximately 80% of the total HSC pool as compared to approximately 20% at baseline (Extended Data Fig. 4a–c; see Supplementary Note 3 for validation of CD150^{high} as a marker for myHSCs after acute LPS treatment)[54]. However, regeneration of myHSCs, MPP2 and MPP3 in the absence of Sema4A was markedly impaired, as the frequency and the absolute number of myHSCs and MPP2 were significantly lower in Sema4AKO mice compared to WT controls (Fig. 4b and Extended Data Fig. 4d). Notably, Sema4AKO myHSCs displayed exaggerated proliferative response to LPS (Fig. 4c). Given that increased HSC proliferative activity during acute inflammatory stress is known to cause a shift from self-renewing to asymmetric/differentiating divisions[55], these results suggest that, in the absence of Sema4A, increased myHSC cycling resulted in depletion of myHSCs through excessive differentiation.

To further test this hypothesis, we performed RNA-seq of myHSCs from WT and Sema4AKO mice 72 h after LPS injection. Similar to changes in aged Sema4AKO myHSC, several key molecules that 'sense' inflammation (*EGR1* and AP-1 family members *Jun*, *Fos* and *MafB*) and mark myeloid differentiation (*CD69* and *LGMN*) were upregulated in 'inflamed' Sema4AKO myHSCs (Fig. 4d)[32–35]. Notably, we also observed a higher expression of *Ndn*, a known *p53* target gene and Fanconi anemia genes *FancI* and *FancF*, consistent with inflammation-induced activation of DNA repair pathways[55]. Interestingly, *HLF* and several genes in the autophagy pathway (A*tg14* and *MAP1LC3B*), which are known to promote HSC self-renewal[56,57], were downregulated, in keeping with a shift toward differentiation. GSEA revealed that, compared to WT myHSCs, Sema4AKO myHSCs displayed significant upregulation of pathways involved in inflammatory response, cell cycle and DNA repair (Fig. 4e). Collectively, our data demonstrate that the absence of Sema4A during acute inflammation results in increased myHSC proliferative stress and excessive activation of the myeloid differentiation program, which likely account for failed myHSC regeneration.

Sema4AKO myHSCs lose self-renewal during chronic inflammation

We next turned to a chronic LPS treatment model (30-d LPS treatment via an intra-peritoneal pump) to assess the functional impact of Sema4A absence on myHSCs in the inflammatory setting. Doing so in an acute LPS treatment model was not feasible due to poor engraftment of rapidly proliferating myHSCs[58].

Overall, we found that phenotypic and functional abnormalities in chronic LPS-treated Sema4AKO mice were greater than those present in these animals at the steady state. In particular, thrombocytosis was more pronounced, and changes in the hematopoietic stem and progenitor cell (HSPC) compartment were more extensive, including expansion of MPP2 and c-Kit$^+$ myeloid-biased progenitors (Fig. 4f–h). Similarly, upon transplantation, prior chronic LPS treatment caused a more prominent increase in Sema4AKO myHSC-derived multi-lineage chimerism, which rapidly (by week 8) reached the approximately 90% mark (Fig. 4i–k). Sema4AKO myHSCs from chronic LPS-treated mice also had a compromised myeloid reconstitution potential, as evidenced by a lower myeloid/lymphoid ratio (Fig. 4l). Secondary transplantation experiments revealed that, in contrast to exaggerated output in primary transplant recipients, Sema4AKO myHSCs generated much lower level of post-transplant chimerism in secondary recipient mice, indicating a

Fig. 3 | The absence of Sema4A in young animals leads to selective myHSC hyperactivation at the steady state. a, Baseline peripheral blood counts of WT and Sema4AKO mice ($n = 7$ mice per group). **b**–**d**, Absolute number of primitive hematopoietic cells (**b**), myHSCs and lyHSCs (**c**) and mature myeloid cells (**d**) in WT/Sema4AKO mice ($n = 6$ mice per group). **e**,**f**, Volcano plots showing DEGs in myHSCs (**e**) and lyHSCs (**f**) from WT and Sema4KO mice. The *x* and *y* axes indicate the expression FC ($\log_2$) and the FDR ($-\log_{10}$) for each gene versus controls, respectively. Legends highlight upregulated (red) or downregulated (blue) transcripts as well as genes not passing cutoff criteria for FC (black) and FDR (gray). Selected representative genes are shown ($n = 4$ biological replicates per genotype). **g**, GSEA showing top overrepresented canonical pathways that are upregulated (red) or downregulated (blue) in Sema4AKO myHSCs as compared to WT myHSCs. The pathways with FDR < 0.05 are shown ($n = 4$ biological replicates per genotype). **h**–**j**, Experimental schema (**h**), overall percentage of donor-derived peripheral blood cells (8 weeks, $P = 0.047$; 12 weeks, $P = 0.02$; 16 weeks, $P = 0.009$; 20 weeks, $P = 0.007$; 24 weeks, $P = 0.003$) (**i**) and lineage contribution by donor-derived cells (B cells: 8 weeks, $P = 0.02$; 12 weeks, $P = 0.01$; 16 weeks, $P = 0.007$; 20 weeks, $P = 0.005$; 24 weeks, $P = 0.003$; T cells: 12 weeks, $P = 0.03$; 16 weeks, $P = 0.03$; 20 weeks, $P = 0.03$; 24 weeks, $P = 0.02$) (**j**) in WT mice (CD45.1), which were competitively transplanted with WT/Sema4AKO myHSCs (CD45.2) ($n = 5$ mice per group). **k**–**m**, Experimental schema (**k**), overall percentage of donor-derived peripheral blood cells (8 weeks, $P = 0.049$; 12 weeks, $P = 0.03$; 16 weeks, $P = 0.046$) (**l**) and lineage contribution by donor-derived cells (myeloid cells: 8 weeks, $P = 0.008$; B cells: 12 weeks, $P = 0.02$; 16 weeks, $P = 0.02$) (**m**) in WT mice (CD45.1), which were competitively transplanted with WT/Sema4AKO lyHSCs (CD45.2) ($n = 4$ mice per group). **n**, Frequency of LT-HSCs (as percentage of Lin$^-$Kit$^+$Sca1$^+$ cells) in the bone marrow of WT mice (CD45.1) after competitive transplantation of WT/Sema4AKO myHSCs (myHSC recipients, CD45.2) and WT/Sema4AKO lyHSCs (lyHSC recipients, CD45.2); quantification and representative plots are shown ($n = 5$ for myHSC recipient groups and $n = 4$ for lyHSC recipient groups). **o**, Myeloid/lymphoid ratio of peripheral blood donor-derived cells in WT mice that were competitively transplanted with WT/Sema4AKO myHSCs ($n = 5$ mice per group). *P* values are shown. For the transplant experiments, $^*P < 0.05$ and $^{**}P < 0.01$. Statistical significance was assessed by two-tailed *t*-test. Mean ± s.e.m. values are shown. BM, bone marrow; LKS, Lin$^-$c-Kit$^+$Sca-1$^+$; PB, peripheral blood.

https://doi.org/10.1038/s43587-024-00798-7

severe self-renewal defect (Fig. 4m,n). Taken together, our results reveal that the absence of Sema4A markedly compromises myHSC resilience to chronic inflammatory stress, leading to functional exhaustion, thus closely resembling the aged Sema4AKO myHSC phenotype.

PlxnD1 is a functional receptor for Sema4A on myHSCs

Because Sema4A is an extrinsic factor, we next sought to identify its cell surface receptor on myHSCs. Sema4A is known to signal via several cell surface receptors across different cell types[26]. Analysis of published LT-HSC gene expression data[59] demonstrated that Plexin B2 (PlxnB2), PlxnD1 and Nrp1, a co-receptor for PlxnD1, displayed the most robust expression (Fig. 5a). Although PlxnB2 was expressed at a higher level than PlxnD1, it was thought to be an unlikely candidate receptor for Sema4A for the following reasons. First, several features of the hematopoietic phenotype of animals deficient in PlxnB2 or another PlxnB2 ligand, Angiogenin, were the opposite of the Sema4AKO phenotype[25,60].

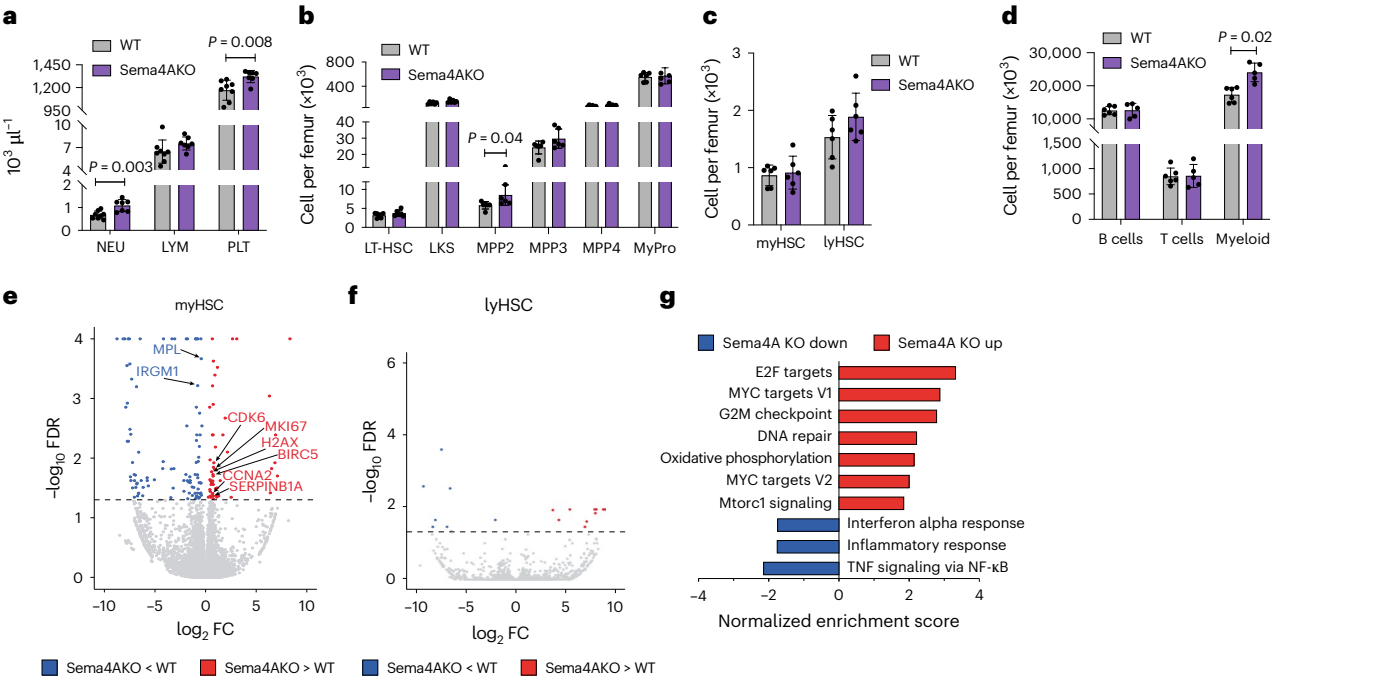

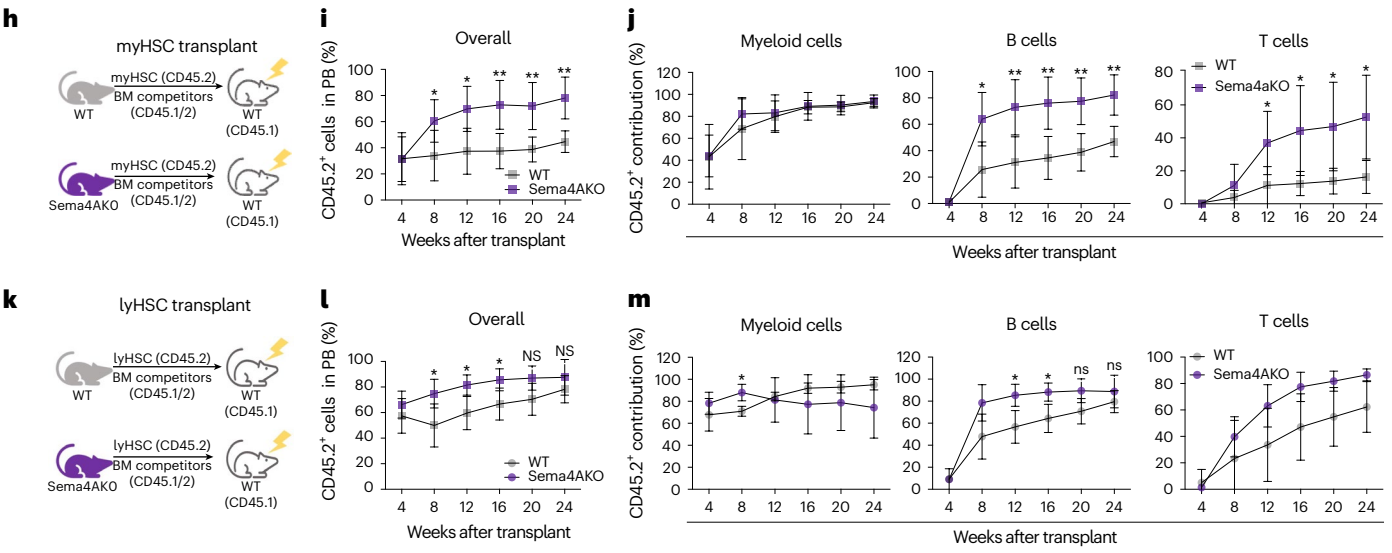

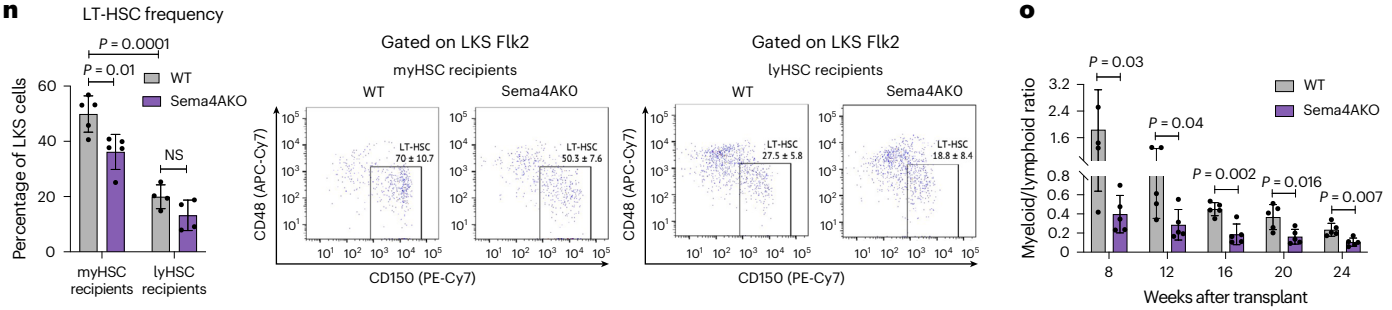

https://doi.org/10.1038/s43587-024-00798-7

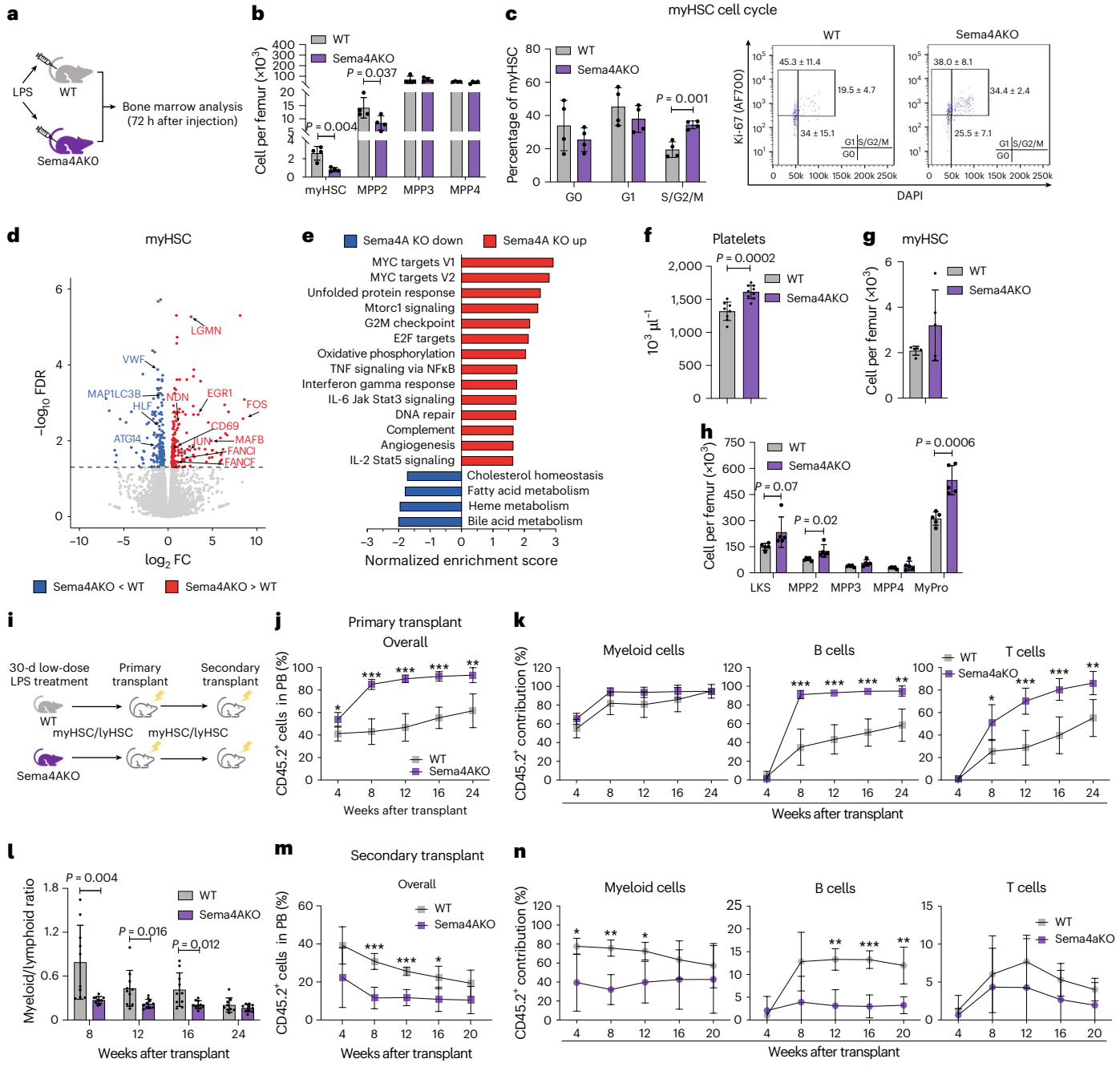

Fig. 4 | Sema4AKO myHSCs are hypersensitive to acute innate immune activation. a–**c**, Experimental schema (**a**), absolute number of myHSCs and progenitor subsets (**b**) and myHSC cell cycle analysis (**c**) in WT/Sema4AKO mice 72 h after LPS injection ($n = 4$ mice per group). **d**, Volcano plot representation of the RNA-seq data from WT/Sema4AKO myHSCs 72 h after LPS injection ($n = 4$ mice per group). **e**, GSEA of myHSCs from WT/Sema4AKO mice 72 h after LPS injection ($n = 4$ mice per group). **f**–**h**, Peripheral blood platelet count (**f**), absolute number of myHSCs (**g**) and primitive hematopoietic cells in WT/Sema4AKO mice (**h**) 30 d after treatment with low-dose LPS ($n = 5$ mice per group). **i**–**k**, Experimental schema (**i**), overall percentage of donor-derived peripheral blood cells (4 weeks, $P = 0.02$; 8 weeks, $P = 5.8 \times 10^{-5}$; 12 weeks, $P = 6.5 \times 10^{-5}$; 16 weeks, $P = 4.8 \times 10^{-5}$; 24 weeks, $P = 0.004$) (**j**) and lineage contribution by donor-derived cells (B cells: 8 weeks, $P = 0.0002$; 12 weeks, $P = 0.0001$; 16 weeks, $P = 0.0001$; 24 weeks, $P = 0.003$; T cells: 8 weeks, $P = 0.02$; 12 weeks, $P = 0.001$; 16 weeks, $P = 0.001$; 24 weeks, $P = 0.01$) (**k**) in primary recipient WT mice (CD45.1), which were competitively transplanted with myHSCs from low-dose LPS-treated WT/Sema4AKO (CD45.2) mice ($n = 5$ mice per group). **l**, Myeloid/lymphoid ratio of donor-derived cells in WT mice (CD45.1), which were competitively transplanted with myHSCs from low-dose LPS-treated WT/Sema4AKO (CD45.2) mice ($n = 5$ mice per group). **m**,**n**, Overall percentage of donor-derived peripheral blood cells (8 weeks, $P = 0.0008$; 12 weeks, $P = 0.0006$; 16 weeks, $P = 0.03$) (**m**) and lineage contribution by donor-derived cells (myeloid cells: 4 weeks, $P = 0.045$; 8 weeks, $P = 0.002$; 12 weeks, $P = 0.03$; B cells: 12 weeks, $P = 0.002$; 16 weeks, $P = 0.0003$; 20 weeks, $P = 0.003$) (**n**) in secondary recipient WT mice (CD45.1), which were competitively transplanted with myHSCs from primary recipient mice (CD45.2) as shown in **i** ($n = 5$ mice per group). *P* values are shown. For the transplant experiments, $^*P < 0.05$ and $^{**}P < 0.01$. Statistical significance was assessed by two-tailed *t*-test. Mean ± s.e.m. values are shown. LKS, $Lin^-c\text{-}Kit^+Sca\text{-}1^+$; PB, peripheral blood.

https://doi.org/10.1038/s43587-024-00798-7

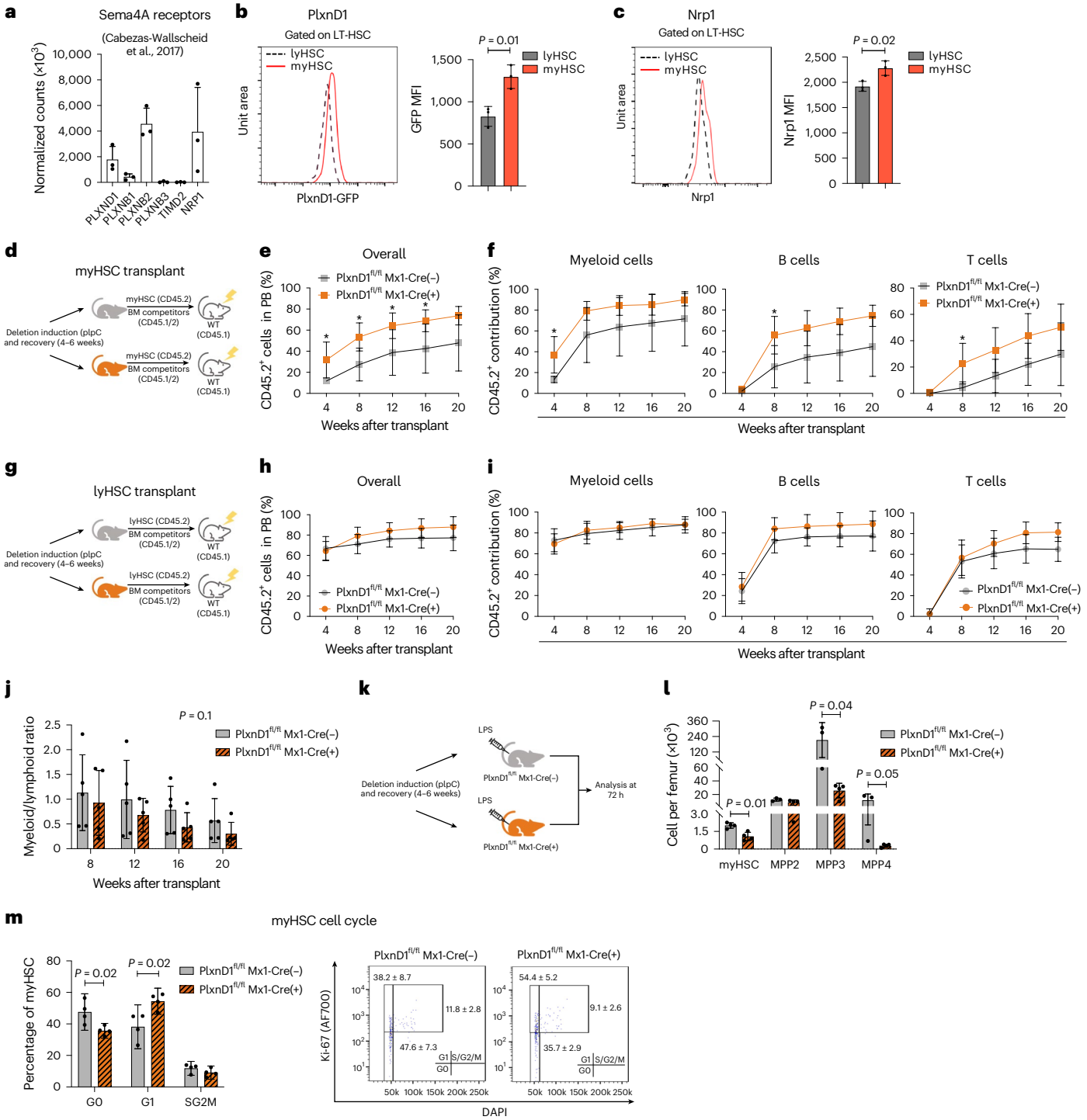

Fig. 5 | PlxnD1 is a functional receptor for Sema4A on myHSCs. a, Expression of mRNA encoding for known Sema4A receptors in HSCs ($n = 3$ mice) (taken from Cabezas-Wallscheid et al.[59]). **b**,**c**, Expression of PlxnD1-GFP reporter (**b**) and Nrp1 protein (**c**) in myHSCs and lyHSCs in WT mice, as assessed by flow cytometry ($n = 3$ biological replicates). **d**–**f**, Experimental schema (**d**), overall percentage of donor-derived peripheral blood cells (4 weeks, $P = 0.03$; 8 weeks, $P = 0.02$; 12 weeks, $P = 0.05$; 16 weeks, $P = 0.05$) (**e**) and lineage contribution by donor-derived cells (myeloid cells: 4 weeks, $P = 0.02$; B cells: 8 weeks, $P = 0.04$; T cells: 8 weeks, $P = 0.03$) (**f**) in WT mice (CD45.1) transplanted with myHSCs from untreated PlxnD1$^{fl/fl}$ Mx1-Cre(+) and PlxnD1$^{fl/fl}$ Mx1-Cre(−) mice (CD45.2) ($n = 5$ mice per group). **g**–**i**, Experimental schema (**g**), overall percentage of donor-derived peripheral blood cells (**h**) and lineage contribution by donor-derived cells (**i**) in WT mice (CD45.1) transplanted with lyHSCs from untreated PlxnD1$^{fl/fl}$ Mx1-Cre(+) and PlxnD1$^{fl/fl}$ Mx1-Cre(−) mice (CD45.2) ($n = 5$ mice per group). **j**, Myeloid/lymphoid ratio of donor-derived cells in WT mice (CD45.1) transplanted with myHSCs from PlxnD1$^{fl/fl}$ Mx1-Cre(+) and PlxnD1$^{fl/fl}$ Mx1-Cre(−) mice (CD45.2) ($n = 5$ mice per group). Overall statistical significance was assessed by two-tailed ANOVA. **k**–**m**, Experimental schema (**k**), absolute number of myHSCs and progenitor subsets (**l**) and myHSC cell cycle analysis (**m**) in PlxnD1$^{fl/fl}$ Mx1-Cre(+) and PlxnD1$^{fl/fl}$ Mx1-Cre(−) mice 72 h after LPS injection ($n = 4$ mice per group). P values are shown. For the transplant experiments, $^{*}P < 0.05$ and $^{**}P < 0.01$. Statistical significance was assessed by two-tailed t-test unless otherwise stated. Mean ± s.e.m. values are shown. BM, bone marrow; PB, peripheral blood.

For example, PlxnB2/AngKO mice displayed lower HSC post-transplant reconstitution and increased lymphoid bias with age, whereas HSC post-transplant reconstitution was increased in Sema4AKO mice, and their hematopoiesis was heavily myeloid biased. Second, the level of PlxnB2 expression did not differ between myHSCs and lyHSCs, and the percentage of PlxnB2$^+$ myHSCs was slightly lower than PlxnB2$^+$ lyHSCs, which would be difficult to reconcile with the myHSC-selective effect of Sema4A (Extended Data Fig. 5a,b). In contrast, both PlxnD1 and Nrp1 showed a higher level of expression in myHSCs compared to lyHSCs at the steady state, and their expression increased further during acute LPS-induced inflammation—a physiological context where Sema4A plays an important myHSC regulatory role (Fig. 5b,c and Extended Data Fig. 5c,d). Notably, analysis of published data from patients with sepsis showed that the frequency of circulating PlxnD1$^+$CD34$^+$ HSPCs and myeloid progenitors (but not lymphoid progenitors) was markedly increased (Extended Data Fig. 5e)[61]. This indicates that, in both mice and humans, PlxnD1 is upregulated during acute inflammatory response and, thus, may be functionally relevant. Hence, we prioritized PlxnD1 for further validation.

Global deletion of PlxnD1 in mice is embryonic lethal due to structural cardiac and vascular defects, thus precluding functional analysis of adult HSCs from these animals[62]. We, therefore, conditionally deleted PlxnD1 by crossing PlxnD1 'floxed' mice[63] with the Mx1-Cre strain. We confirmed a complete excision of PlxnD1 by polymerase chain reaction (PCR) and quantitative PCR (qPCR) analysis of sorted Lin$^-$Kit$^+$Sca$^+$ cells after polyinosine-polycytidylic acid (poly I:C) induction (Extended Data Fig. 5f,g). Analysis of peripheral blood and the bone marrow of PlxnD1$^{fl/fl}$ Mx1-Cre(+) and PlxnD1$^{fl/fl}$ Mx1-Cre(−) mice at the steady state showed no abnormalities (Extended Data Fig. 5h–l). However, competitive transplantation experiments revealed that, similar to the behavior of myHSCs/lyHSCs from Sema4AKO mice, myHSCs from PlxnD1$^{fl/fl}$ Mx1-Cre(+) donors generated a higher level of multi-lineage chimerism compared to PlxnD1$^{fl/fl}$ Mx1-Cre(−) controls, whereas PlxnD1$^{fl/fl}$ Mx1-Cre(+) and PlxnD1$^{fl/fl}$ Mx1-Cre(−) lyHSCs displayed equivalent engraftment levels (Fig. 5d–i). Assessment of graft lineage composition revealed that, especially at later timepoints, PlxnD1-deficient myHSCs displayed a lower myeloid/lymphoid ratio (similar to Sema4A myHSCs), although the difference did not reach statistical significance (Fig. 5j; $P = 0.1$ by ANOVA). Post-transplant bone marrow analysis at week 20 demonstrated that PlxnD1 deletion in myHSCs (unlike Sema4A deletion) had no measurable impact on the frequency of myHSC-derived HSCs and MPP4 (Extended Data Fig. 5m,n). However, the level of MPP4 Flk2 expression in the PlxnD1-deleted cohort was higher and consistent with a shift toward lymphoid differentiation, as seen in the Sema4AKO model (Extended Data Fig. 5o). Notably, PlxnD1 deletion was inconsequential for lyHSC differentiation (Extended Data Fig. 5m–o). Cumulatively, these results show that, although the impact of PlxnD1 deletion on myHSCs was somewhat less pronounced than that of Sema4A, it recapitulates the key aspect of the Sema4AKO phenotype.

Given the role of Sema4A in attenuating myHSC sensitivity to acute LPS-induced inflammatory stress, we asked if PlxnD1 deletion phenocopies that of Sema4AKO in this experimental model. We found that, at 72 h after LPS injection, PlxnD1-deficient myHSCs excessively proliferated, became depleted in number and generated fewer downstream multipotent progenitors, thus largely recapitulating the Sema4AKO phenotype (Fig. 5k–m and Extended Data Fig. 5p). These results demonstrate that, like the absence of Sema4A, the absence of PlxnD1 enhances the sensitivity of myHSCs to acute inflammatory stress and compromises their regenerative function.

In sum, these results support our hypothesis that PlxnD1 serves as a receptor for Sema4A on myHSCs. However, we cannot rule out that other cell surface molecules and, in particular, Nrp1, a co-receptor for PlxnD1, are involved in transmitting myHSC-directed Sema4A signals.

The effect of Sema4A is non-cell-autonomous

In the next set of experiments, we investigated whether Sema4A acts as a cell-autonomous—that is, myHSC derived—or a cell-non-autonomous regulator. Examination of Sema4A expression in the bone marrow at baseline (as well as during acute inflammation and aging) showed that, in myHSCs, Sema4A mRNA and protein levels were low/undetectable; in contrast, Sema4A was abundantly expressed in granulocytes and monocytes (Extended Data Fig. 6a,b), which served as predominant sources of Sema4A in the bone marrow (Fig. 6a and Extended Data Fig. 6c). Such an expression pattern suggests that Sema4A likely acts as a non-cell-autonomous, myHSC-extrinsic regulator.

To investigate the effect of global microenvironmental deletion of Sema4A on myHSCs, we first performed intravital microscopy of transplanted WT myHSCs in lethally irradiated WT/Sema4AKO animals. We transferred an equal number of WT myHSCs (which had been fluorescently labeled ex vivo) and imaged these cells in the calvarial bone marrow of live mice 24 h later (Fig. 6b). Notably, the number of transplanted cells in the Sema4AKO-deficient hosts was significantly higher, consistent with their faster proliferation (Fig. 6c and Extended Data Fig. 6d), which is similar to what we found in non-transplanted Sema4AKO animals (Fig. 4c and Extended Data Fig. 3a). Interestingly, flow cytometry showed that, at 24 h after irradiation, neutrophils became the main source of Sema4A in the bone marrow, contributing to almost 90%, and that neutrophil expression of Sema4A on a per-cell basis was also increased (Extended Data Fig. 6e).

Next, we analyzed long-term reconstitution kinetics of WT myHSCs in WT/Sema4A-deficient bone marrow microenvironment using the same experimental setting. We found that Sema4AKO recipients developed anemia, neutrophilia in the peripheral blood as well as myHSC expansion and myeloid bias in the bone marrow (Fig. 6d–f)—that is, the features that were also present in Sema4AKO mice, particularly during aging (Figs. 1a–c and 3a,d). Collectively, the transplantation and imaging experiments show that pan-cellular deletion of Sema4A in the host bone marrow microenvironment is sufficient to recapitulate the key aspects of the Sema4AKO phenotype.

Neutrophils are an indispensable source of Sema4A

Having established that Sema4A acts in a non-cell-autonomous fashion, we next focused on granulocytes as a predominant cellular source of Sema4A. We observed that Sema4A$^+$ expression was particularly high in the mature (Ly6G^{high})[64] neutrophil fraction (Fig. 6g and Extended Data Fig. 6f). To directly test the impact of neutrophil-derived Sema4A on myHSCs, we crossed Sema4A 'floxed' mice with the Mrp8-Cre strain[65]. We observed Cre-mediated excision in over 90% of neutrophils (Extended Data Fig. 6g), consistent with the published data[66]. At baseline, Sema4A$^{fl/fl}$ Mrp8-Cre(+) mice had no phenotypic hematopoietic abnormalities (Extended Data Fig. 6h–j). We, therefore, examined the phenotype of these mice under acute and chronic inflammatory conditions. After acute LPS challenge, Sema4A$^{fl/fl}$ Mrp8-Cre(+) mice displayed exaggerated response, as evidenced by reduced frequency and the absolute number of MPPs (but not myHSCs) (Fig. 6h,i and Extended Data Fig. 6k,l), mirroring major findings in straight Sema4AKO and PlxnD1KO strains. Moreover, after chronic LPS treatment, transplanted myHSCs from Sema4A$^{fl/fl}$ Mrp8-Cre(+) mice displayed similar behavior to that of straight Sema4AKO myHSCs—that is, lymphoid skewing, reduced self-renewal and enhanced production of lymphoid-biased MPP4 (Fig. 6j–m and Extended Data Fig. 6m,n).

Collectively, these findings demonstrate that neutrophils serve as a physiologically important, non-redundant cellular source of Sema4A in the bone marrow niche. Given that neutrophils are a direct progeny of myHSCs, our data suggest the existence of a feedback loop whereby neutrophils safeguard their own production by maintaining inflammation resilience and 'lineage fidelity' of myHSCs.

https://doi.org/10.1038/s43587-024-00798-7

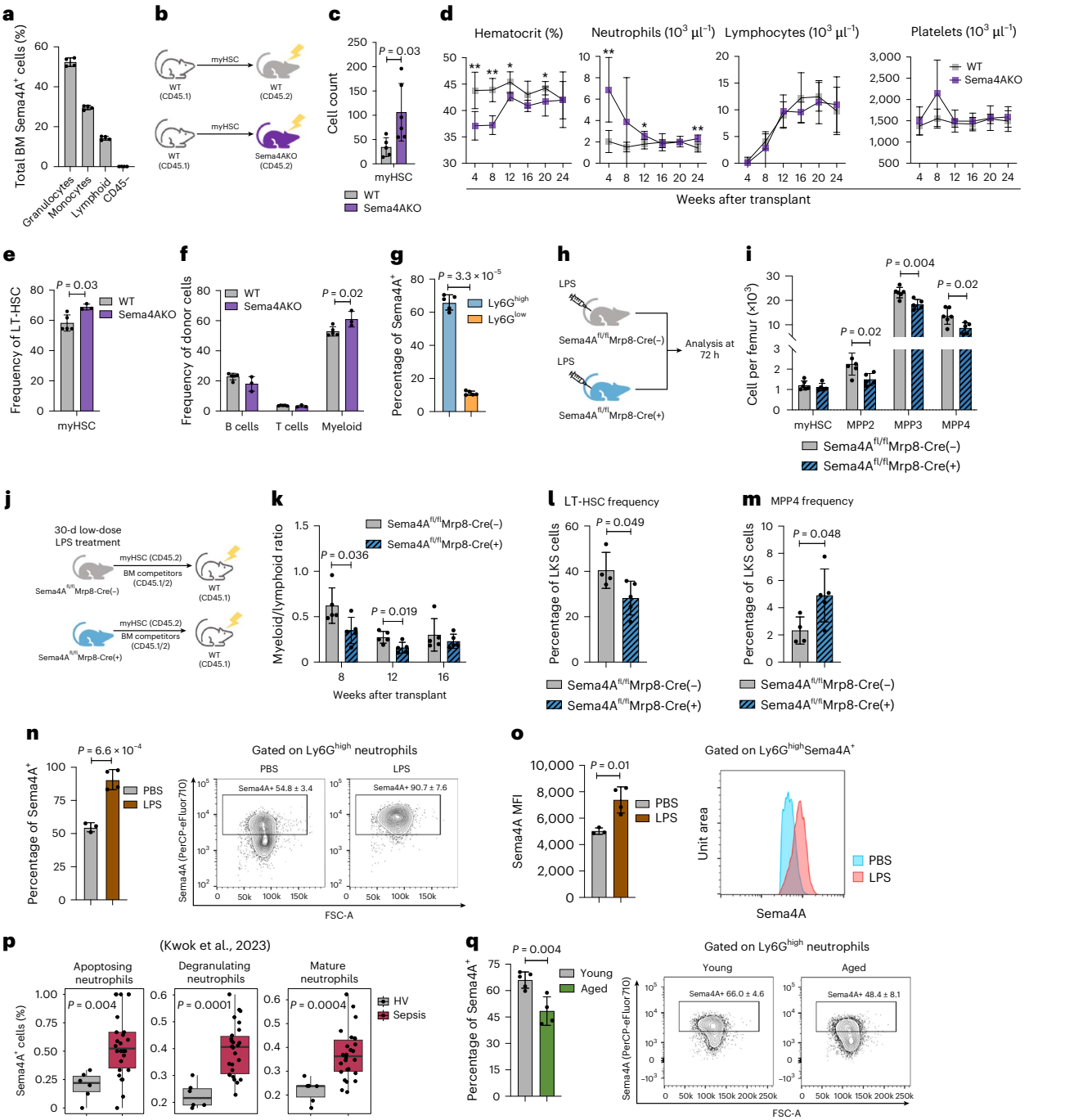

Fig. 6 | Neutrophils serve as a physiologically important source of Sema4A. **a**, Relative contribution of distinct cellular subsets to Sema4A production in the bone marrow at the steady state ($n = 4$ mice per group). **b**,**c**, Experimental schema for non-competitive transplantation of WT myHSCs into lethally irradiated WT/Sema4AKO recipients (**b**) and the number of transplanted myHSC progeny in calvarial bone marrow, as assessed by intravital microscopy at the 24-h timepoint (**c**) ($n = 4$ mice per group). **d**–**f**, Longitudinal blood counts (hematocrit: 4 weeks, $P = 0.004$; 8 weeks, $P = 0.005$; 12 weeks, $P = 0.02$; 20 weeks, $P = 0.04$; neutrophils: 4 weeks, $P = 0.001$; 12 weeks, $P = 0.01$; 24 weeks, $P = 0.002$) (**d**), donor-derived LT-HSC frequency (**e**) and mature cell frequency (**f**) in the bone marrow of a separate WT/Sema4AKO cohort, which was non-competitively transplanted with WT myHSCs ($n = 5$ mice for the WT group and n = 3 mice for the Sema4AKO group) (**g**). Sema4A expression in Ly6G^{high} versus Ly6G^{low} neutrophils ($n = 5$ mice per group). **h**,**i**, Experimental schema (**h**) and absolute number of myHSCs and primitive hematopoietic cells (**i**) in Sema4A$^{fl/fl}$ Mrp8-Cre(+) and Sema4A$^{fl/fl}$ Mrp8-Cre(−) mice 72 h after LPS injection ($n = 5$ mice per group). **j**–**m**, Experimental schema (**j**), myeloid/lymphoid ratio of peripheral blood donor-derived cells (**k**), donor-derived LT-HSC frequency (**l**) and donor-derived MPP4 frequency (**m**) in WT mice (CD45.1), which were competitively transplanted with myHSCs from low-dose LPS-treated Sema4A$^{fl/fl}$ Mrp8-Cre(+) and Sema4A$^{fl/fl}$ Mrp8-Cre(−) (CD45.2) mice ($n = 5$ mice per group). **n**,**o**, Sema4A expression in bone marrow WT Ly6G^{high} neutrophils 24 h after LPS injection, as quantified by frequency of Sema4A$^+$ cells (**n**) and Sema4A mean fluorescence intensity (MFI) of Sema4A$^+$ Ly6G^{high} neutrophils ($n = 4$ mice per group). Bar graph and representative flow cytometry plots are shown. **p**, Frequency of Sema4A$^+$ cells in peripheral blood neutrophil subsets from patients with sepsis and healthy volunteers (HVs), as assessed by single-cell RNA-seq in Kwok et al.[61]. Displayed is a cumulative analysis of 'non-zero' PlxnD1 expression values in single HSPCs obtained from 26 patients with sepsis and six HVs. The plots show the median (middle line), interquartile range (box) and minimum to maximum values (whiskers) throughout. **q**, Frequency of Sema4A$^+$ Ly6G^{high} neutrophils in the bone marrow of young and aged WT mice ($n = 5$ mice for the young WT group and $n = 4$ mice for the aged WT group). P values are shown. For the transplant experiments, $^*P < 0.05$ and $^{**}P < 0.01$. Statistical significance was assessed by two-tailed t-test. Mean ± s.e.m. values are shown. BM, bone marrow; FSC-A, forward scatter area; LKS, Lin$^-$c-Kit$^+$Sca-1$^+$.

Inflammation and aging alter Sema4A expression in neutrophils

In the next set of experiments, we asked whether changes in neutrophil Sema4A expression also occur during inflammation and aging, which would link our findings in the genetic knockout models to a potential role of Sema4A in normal physiological settings. Interestingly, we discovered that, in mice, both the frequency of Sema4A$^+$ neutrophils within the Ly6G^{high} fraction and their level of Sema4A expression markedly increased after acute treatment with LPS (Fig. 6n,o). Similarly, in humans with sepsis, the frequency of Sema4A$^+$ neutrophils across several neutrophil subsets, including mature neutrophils—but not in lymphoid cells—also became significantly elevated (Fig. 6p and Extended Data Fig. 6o)[61]. Surprisingly, Sema4A expression in neutrophils during aging revealed the opposite pattern: the frequency of Sema4A$^+$ neutrophils within Ly6G^{high} fraction declined and the level of Sema4A expression also diminished as compared to young animals (Fig. 6q and Extended Data Fig. 6p). Given our findings that a total absence of Sema4A leads to premature hematopoietic aging-like phenotype, this observation raises the possibility that age-related decrease in neutrophil-derived Sema4A triggers physiological hematopoietic aging.

Sema4A maintains the epigenetic identity of myHSCs

The data from multiple models employed in our study reveal that Sema4AKO myHSCs display inferior self-renewal and lymphoid-skewed post-transplant differentiation as compared to myHSCs from controls. Intriguingly, the same features characterize WT lyHSCs when compared to WT myHSCs[12,67]. A recent study by Meng et al.[68] showed that, in case of WT lyHSC/WT myHSCs, the functional differences between the two HSC subsets are closely linked to their distinct epigenetic signatures. We, therefore, hypothesized that a similar, epigenetically driven mechanism may explain the functional differences between WT and Sema4AKO myHSCs that we observed.

To test this hypothesis, we performed assay for transposase-accessible chromatin with high-throughput sequencing (ATAC-seq) profiling of these cells from aged WT/Sema4AKO mice. Assessment of the chromatin accessibility using principal component analysis (PCA) showed that PC1 distinguishes the genome-wide ATAC-seq profiles of aged Sema4AKO myHSCs from those of aged WT myHSCs (Fig. 7a). Consistent with this, we detected 242 ATAC-seq peaks or open chromatin regions (OCRs) with an increase in signal and 144 OCRs with a decrease in signal in the aged myHSC ATAC-seq profiles compared to those of aged WT myHSCs (Fig. 7b). Thus, Sema4AKO myHSCs appear to be epigenetically distinct from WT myHSCs.

As mentioned above, Sema4AKO myHSCs display an lyHSC-like in vivo behavior. To determine whether the changes that we observed in Sema4AKO myHSCs make them epigenetically more similar to lyHSCs, we first generated a WT lyHSC ATAC-seq signature. Specifically, we compiled a list of differentially regulated genes with upstream regulator elements (UREs) within 1–50 kb from the transcription start site that showed increased accessibility in aged WT lyHSCs (which we also profiled) as compared to aged WT myHSCs. As expected, our lyHSC ATAC-seq signature was strongly enriched in genes that were previously identified by Meng et. al.[68] when WT lyHSCs (referred to as MUL HSCs) and WT myHSCs (referred to as PLT HSCs) were compared by ATAC-seq profiling (Fig. 7c, left panel). Furthermore, we observed a similar enrichment of this lyHSC ATAC-seq gene signature in genes that showed an increased accessibility of the URE in Sema4AKO myHSCs as compared to WT myHSCs (Fig. 7c, right panel). These results indicate that functional distinctions between WT myHSCs/WT lyHSCs and WT myHSCs/Sema4AKO myHSCs with respect to self-renewal and lineage bias are likely driven by a shared epigenetic mechanism. However, the global difference between Sema4AKO myHSCs and WT myHSCs may be less pronounced than the difference between WT myHSCs and WT lyHSCs where we found a larger number of differentially regulated OCRs (2,654 and 2,225, respectively).

Next, we performed motif enrichment analysis to identify DNA-binding transcription factors that may be alerted and contribute to changes in the epigenetic programming of the myHSC pool in response to the loss of Sema4AKO. Among our top hits in the accessible regions in the Sema4AKO myHSCs were motifs that matched the preferred binding sites of the transcription factors PRDM15, CREB1, TFDP1, RUNX3 and SPIC (Fig. 7d). In addition, we found that Runx3 transcription was significantly upregulated in myHSCs in the Sema4AKO condition, based on our single-cell RNA-seq analysis (Fig. 7e). Interestingly, the study of WT lyHSCs/myHSCs by Meng et al.[68] found that binding sequences for RUNX3—a chromatin pioneer factor that acts as a master regulator of HSC lymphoid bias[69]—were highly enriched in the accessible chromatin of WT lyHSCs and that *Runx3* mRNA level in lyHSCs was higher. Thus, WT lyHSCs and Sema4AKO myHSCs share not only the global features of WT lyHSC epigenetic signature but also specific molecules that regulate their chromatin state.

Taken together, our data highlight the critical role of Sema4A in maintaining the epigenetic identity of myHSCs. In the absence of Sema4A, the epigenetic distinctions between myHSCs and lyHSCs become blurred, and myHSCs start to functionally resemble lyHSCs, leading to the loss of diversity within the total HSC pool.

Discussion

In this work, we define Sema4A as a previously unrecognized cell-extrinsic hematopoietic regulator that selectively protects a specialized stem cell subset—myHSCs—from inflammation-induced injury. Although prior studies suggested that myHSCs may rely on dedicated signals to preserve their function[11,52,70], those that are important in the context of inflammatory stress—to which myHSCs are most vulnerable—have not, to our knowledge, been previously identified. We show here that the protective role of Sema4A is functionally relevant across several animal models of inflammation, such as tonic inflammatory stimulation, LPS-induced emergency myelopoiesis and chronic low-dose LPS exposure, but it is most critical during aging.

Our gene expression data show that both 'inflamed' and aged Sema4AKO myHSC signature is dominated by genes that are known to be upregulated in response to inflammatory stress, such as *EGR1*, *Jun* and *Fos*[36]. This indicates that excessive expansion of aged Sema4AKO myHSCs and their subsequent regenerative failure resulted from increased sensitivity to inflammatory cues, which are abundant during 'inflammaging'[43]. In light of recent findings that inflammatory signals drive hematopoietic aging[17], our results demonstrate that when resistance to these signals is compromised—as occurs in the absence of Sema4A—myHSC aging as well as overall hematopoietic aging occur prematurely. Thus, we propose that by protecting myHSCs from inflammatory stress and safeguarding their integrity throughout the animal's lifespan, Sema4A maintains the overall functional diversity of the HSC pool and ensures hematopoietic longevity.

The striking functional deficit of aged Sema4AKO myHSCs that we observed likely stems from myHSC hyperactivation at young age, which is evident from our transcriptomic and functional studies. Interestingly, our experiments in young WT/Sema4AKO animals showed that, in addition to regulating 'generic' myHSC properties, such as self-renewal and multi-lineage reconstitution, Sema4A was also responsible for maintaining two key functional characteristics of myHSCs, namely lower post-transplant output and predominantly myeloid-biased differentiation[71]. We showed that, upon transplantation, Sema4AKO myHSCs lose functional identity, because their level of peripheral donor chimerism and lineage output become similar to that of WT lyHSCs. Although specific molecular mechanisms underlying these findings remain unclear and will be addressed in future studies, it is noteworthy that the 'lyHSC drift' of young Sema4AKO myHSCs correlated with transcriptional evidence for upregulation of oxidative phosphorylation—a metabolic hallmark of lyHSCs, which rely on intact mitochondrial function for maintenance of the lymphoid

https://doi.org/10.1038/s43587-024-00798-7

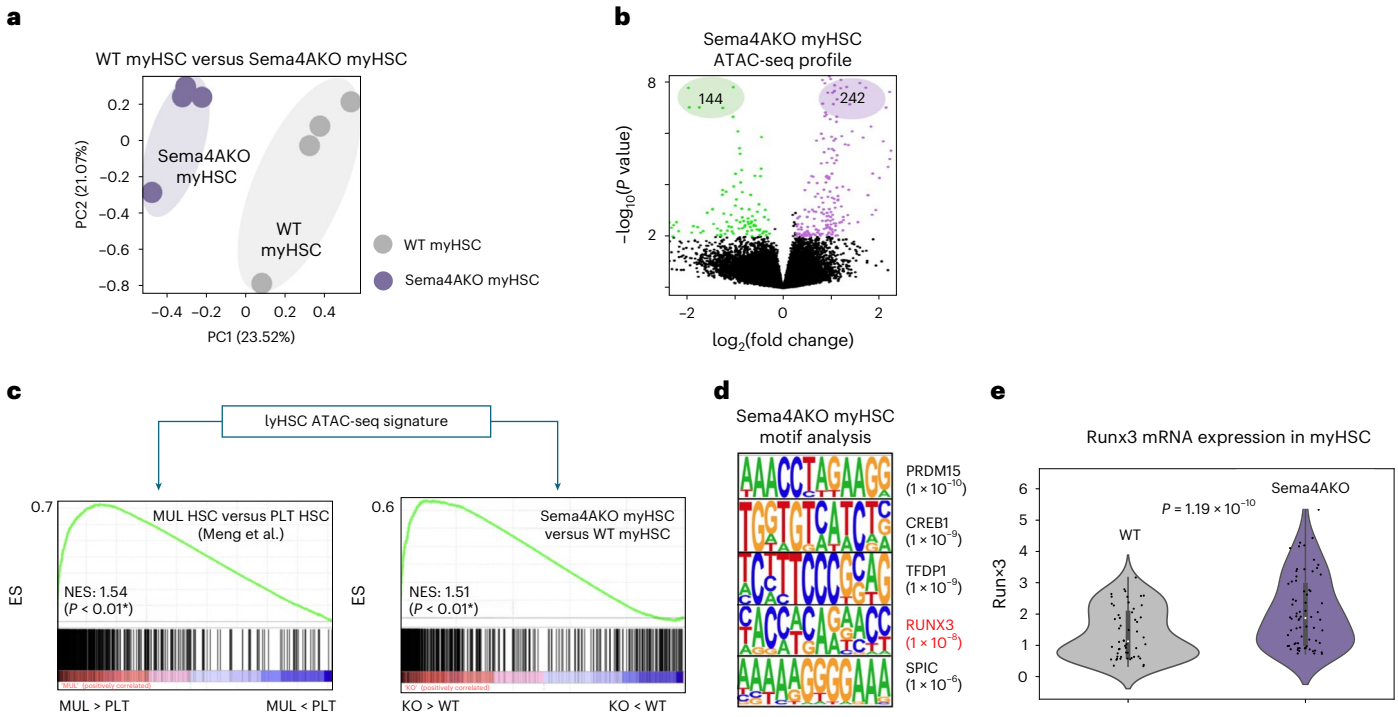

Fig. 7 | Sema4A maintains the epigenetic identity of myHSCs. a, PCA analysis of ATAC-seq signatures of myHSCs from aged WT/Sema4AKO mice. **b**, Volcano plot of OCRs that show increased accessibility ($n = 242$) and decreased accessibility ($n = 144$) in aged Sema4AKO myHSCs ($P < 0.01$ (y axis), by two-sided Wald test). **c**, GSEA of the lyHSC differentially accessible gene signature over the lyHSC gene signature from Meng et al.[68] (MUL versus PLT; left panel) and the Sema4A myHSC accessibility genes (right panel). Note that, in the Meng et al. dataset, MUL and PLT denote lyHSC-comparable and myHSC-comparable HSC subsets, respectively ($P < 0.01$, by one-sided weighted Kolmogorov–Smirnov test). **d**, Enriched de novo motifs predicted from myHSC/Sema4AKO enriched open chromatin ($P < 1 \times 10^{-6}$, by two-sided t-test). **e**, Gene expression level of Runx3 in aged WT/Sema4AKO myHSCs (from RNA-seq data) ($n = 322$ cells across two biological replicates and four technical replicates). In the inner box plots of the violin plots, the white point shows the median value; box limits indicate upper and lower quartiles; and whiskers extend to minimum and maximum values. Statistical significance was assessed by two-tailed Wilcoxon rank-sum test. NES, normalized enrichment score.

differentiation potential[72]. Thus, we hypothesize that by preventing myHSC transition to oxidative phosphorylation, Sema4A may control a metabolic node that is required to maintain the functional myHSC phenotype. Notably, a similar 'metabolic stabilizer' function for Sema4A was previously described in another long-lived cell population—regulatory T cells—where Sema4A prevented overactivation of Akt-mTOR signaling, a key regulator of oxidative phosphorylation and mitochondrial function[27]. Interestingly, excessive mitochondrial metabolism via upregulation of CD38 was recently reported to impair HSC function during aging[73], suggesting that myHSC metabolic hyperactivation in young animals may have contributed to the aged Sema4AKO myHSC phenotype.

We discovered that the effect of Sema4A is non-cell-autonomous and that neutrophils (in particular, their mature Ly6G^{high} fraction) serve as a major cellular source of Sema4A in the bone marrow, although other cell types also contribute. Neutrophil-derived Sema4A likely acts locally, because Gr1^{+} myeloid cells are evenly distributed throughout the marrow, positioned in close proximity (<50 µm) to all c-Kit^{+} HSPCs and are known to serve as a source of paracrine HSC regulatory signals[74,75].

We found that Sema4A expression in Ly6G^{high} neutrophils becomes markedly upregulated after acute inflammatory insult, likely via an NF-κB-mediated mechanism, because Sema4A promoter contains an NF-κB binding site[76]. Given our data that the lack of neutrophil-derived Sema4A impairs myHSC function, this observation suggests that an increase in neutrophil-derived Sema4A expression serves as a myHSC-protective mechanism. We propose that this mechanism operates via a negative feedback loop whereby neutrophils—a direct progeny of myHSCs—secrete Sema4A to prevent inflammation-induced myHSC damage. However, it appears that, during aging, this mechanism fails because Sema4A production by Ly6G^{high} neutrophils decreases due to significant loss of Sema4A-expressing cells within this population. Our data suggest that age-related decrease in neutrophil-derived Sema4A may contribute to physiological myHSC aging, similar to IGF1, as previously reported[77]. Hence, pharmacological restoration of niche-derived signals may offer an opportunity for anti-aging therapeutic intervention[78].

We identified PlxnD1 as a functional receptor for Sema4A on myHSCs. Although this molecule was previously known as a regulator of endothelial and mature immune cells[62,79], its role in hematopoiesis had not, to our knowledge, been previously defined. Our data demonstrate that PlxnD1 serves as an inhibitory receptor on myHSCs and attenuates the intensity of inflammatory response. Similar to Sema4A, PlxnD1 expression is upregulated during acute inflammation and increases in myHSCs in mice and HSCs in humans, thus further enhancing the strength of protective Sema4A signaling. Given that, in some experimental settings, deletion of PlxnD1 resulted in less pronounced changes than deletion of Sema4A, it is likely that PlxnD1 is not the only molecule that transmits Sema4A signals. We hypothesize that PlxnD1 co-receptor Nrp1 (ref. 80) also contributes, because it shows higher expression on myHSCs and is further upregulated in response to acute inflammation.

Finally, we note that, although our study highlights the importance of HSC-directed 'inflammation resistance' signals, such as Sema4A, in mouse inflammatory hematopoiesis, our work may have direct translational relevance to human health. Recent studies showed that, in humans, HSC inflammatory memory (which is epigenetically mediated) underlies hematopoietic and immune defects in aging, clonal hematopoiesis and inflammatory disorders[81]. Thus, reducing HSC inflammation responsiveness via dampening the acquisition of such

a memory would be clinically beneficial. Given that Sema4A serves as an 'inflammation resistance' signal for myHSCs and operates at the chromatin level, as we discovered, recombinant Sema4A protein or small-molecule agonists of Sema4A/PlxnD1 may serve as future therapeutic agents to fulfil this role.

Methods

Experimental model and subject details

Animals. All animal experiments were approved by the Institutional Animal Care and Use Committee at Fred Hutchinson Cancer Center (protocol number 51002). WT C57Bl/6J, B6SJL, Mx1-Cre and Mrp8-Cre mice were obtained from The Jackson Laboratory. PlxnD1 conditional KO mice and PlxnD1-GFP were obtained from Chenghua Gu (Harvard University). Sema4AKO mice were obtained from Atsushi Kumanogoh (University of Osaka)[22]. Sema4A conditional KO mice were obtained from Thomas Worzfeld (University of Marburg). Generation of mice carrying a targeted allele of Sema4A was described previously[82].

To induce conditional deletion via Mx1-Cre, 6–8-week-old mice were interperitoneally injected with 100 µg per mouse of high-molecular-weight poly I:C (InvivoGen) once every other day for a total of three injections and analyzed 4 weeks after the last injection.

For most of the experiments, both male and female animals were used. Each cohort of animals was matched for age and sex. For acute LPS-induced inflammation experiments, only male mice were used. Young mice ranged from 8 weeks to 12 weeks of age, and aged mice ranged from 74 weeks to 80 weeks. For the aging experiments, both male and female cohorts were generated, but only the female cohort was analyzed in detail. Both WT and Sema4AKO mice were aged in the same environment. All mice were housed on a 12-h light/dark cycle at 25 °C. Mice were provided with standard chow (LabDiet, PicoLab Rodent Diet 20, cat. no. 5053) and water ad libitum. Humidity was kept at 30–70%. On-site veterinarians provided health status checks.

PCR genotyping and excision validation for conditional alleles. Genomic DNA was extracted from peripheral blood samples using a DNeasy Blood & Tissue Kit (Qiagen) according to the manufacturer's instruction or using a fast extraction method involving incubation in ACK Lysing Buffer (Gibco) followed by resuspension in 50 mM NaOH, incubation at 95 °C and neutralization with 1 M Tris buffer (pH 7). Genotyping PCR primer sequences are listed in the reagents table.

To confirm Mx1-Cre-mediated excision of PlxnD1 'floxed' allele, up to 50,000 $Lin^-c\text{-}Kit^+Sca\text{-}1^+$ cells from animals of desired genotypes were sorted into 350 µl of RLT Plus Buffer (Qiagen). DNA and RNA were extracted with an AllPrep DNA/RNA Micro Kit (Qiagen) according to the manufacturer's instructions. Primers listed in the reagents table were used to detect the excised and non-excised alleles by genomic DNA PCR. In addition, RNA was reverse transcribed using SuperScript IV VILO Master Mix (Invitrogen), and expression of PlxnD1 exon 1 relative to GAPDH was determined using PowerTrack SYBR Green Master Mix (Applied Biosystems) and qPCR primers listed in the reagents table.

Sema4A qPCR. To quantify Sema4A transcript levels in niche cell subsets and HSCs, 50,000–80,000 $CD45^-$ cells, granulocytes, monocytes and lymphocytes and 2,000–5,000 HSCs were sorted into 350 µl of RLT Plus Buffer (Qiagen). RNA was extracted with the AllPrep DNA/RNA Micro Kit (Qiagen) according to the manufacturer's instructions and was reverse transcribed using SuperScript IV VILO Master Mix (Invitrogen). Expression of Sema4A exon 1 relative to GAPDH was determined using PowerTrack SYBR Green Master Mix (Applied Biosystems) and qPCR primers listed in the reagents table.

Histological analysis. Dissected tissue samples were fixed in 4% formalin for 24 h, decalcified in EDTA for 2 weeks and embedded in paraffin. Tissue sections were stained with hematoxylin and eosin (H&E).

Flow cytometry and cell sorting. Whole bone marrow mononuclear cells (BMMNCs) were collected by crushing tibias, femurs and pelvis in Ca^{2+}/Mg^{2+}-free Dulbecco's phosphate-buffered saline (D-PBS) supplemented with 2% FBS (Thermo Fisher Scientific). Cells were stained with the antibodies listed in the reagents list. Samples were analyzed on a BD FACSymphony A5 (BD Biosciences) or sorted on a BD FACSAria II (BD Biosciences). All flow cytometry data were analyzed using FlowJo software. Graphs were made using GraphPad Prism 9 (GraphPad Software) or Microsoft Excel.

Cell cycle analysis. For cell cycle analysis, we used our published protocol[83]. BMMNCs were stained with conjugated monoclonal antibodies for HSPC markers, as described above. The cells were fixed and permeabilized using a Cytofix/Cytoperm Fixation/Permeabilization Kit (BD Biosciences) according to the manufacturer's instruction. Cells were then stained with fluorescently conjugated Ki67 antibody (1:20; BD Biosciences) for 45 min, followed by 4,6-diamidino-2-phenylindole (1:300; Invitrogen) for 10 min. Samples were analyzed at 2,500–3,000 threshold rate.

BrdU incorportation. For BrdU incorporation, mice were first injected intraperitoneally with BrdU (Sigma-Aldrich) and subsequently put on BrdU drinking water for 4 d before analysis, as previously described[84]. Cells were stained with conjugated monoclonal antibodies for HSPC markers, as described above. Cells were then fixed, permeabilized and stained for BrdU using a FITC BrdU Flow Kit (BD Biosciences) according to the manufacturer's instructions. All samples were analyzed using the BD FACSymphony A5.

Transplantation experiments. For all transplantation experiments, recipients were lethally irradiated 24 h before transplant at 1,200 cGy (a split dose of 600 cGy + 600 cGy with a 3-h interval between doses) and maintained on Baytril-containing water for the first 4 weeks.

For competitive transplantation experiments involving young mice, 200–400 myHSCs ($Lin^-c\text{-}Kit^+Sca\text{-}1^+CD48^-CD34^-Flk2^-CD150^{high}$) or 200–400 lyHSC ($Lin^-c\text{-}Kit^+Sca\text{-}1^+CD48^-CD34^-Flk2^-CD150^{low}$) from CD45.2 C57Bl/6J, Sema4AKO, $PlxnD1^{fl/fl}$ Mx1-Cre and LPS-treated models were co-injected with 200,000–250,000 CD45.1/2 competitor cells. For competitive transplantation experiments using HSCs from aged mice, 2,000 myHSC or 2,000 lyHSC CD45.2 cells were transplanted with 200,000 CD45.1/2 competitor cells. Peripheral blood donor chimerism was monitored at 4-week intervals. Flow cytometry gating strategies for the identification of myHSCs and lyHSCs are shown in Extended Data Fig. 1a.

For the non-competitive transplant experiments, the animals were lethally irradiated (as described above) and injected with 1,100–1,600 WT (CD45.1) myHSCs or lyHSCs. Engraftment kinetics were monitored by blood counts and flow cytometry every 4 weeks.

Post-transplant chimerism analysis. Peripheral blood was collected from each recipient via retro-orbital sinus, and complete blood count (CBC) was performed immediately after blood collection using Element HT5 (HESKA). Red blood cells were lysed in ACK Lysing Buffer (Gibco) and then stained with fluorescently conjugated antibodies listed in the reagents list. Samples were analyzed using the BD FACSymphony A5.

Induction of inflammatory response. To induce chronic inflammation, WT C57Bl/6J and Sema4AKO mice were implanted with an intra-abdominal alzet osmotic pump (Braintree Scientific) that was loaded with LPS (InvivoGen) resuspended in PBS. A dose of 8.4 mg kg^{-1} LPS was administered over a 30-d period.

To induce acute inflammation, mice were injected intraperitoneally with 3.0–4.5 µg g^{-1} (depending on the biological activity of a specific batch, which was established by titration) of LPS (InvivoGen) resuspended in PBS and euthanized at the point of maximal clinical

response, which occurred at 72 h after injection. Bone marrow was analyzed on the BD FACSymphony or sorted on the BD FACSAria II for transplantation experiments.

Intravital imaging. myHSCs and lyHSCs were isolated by flow sorting, as described above. Cells were stained with 10 µM DiD (Invitrogen) in D-PBS supplemented with 2% FBS for 20 min at 37 °C. Approximately 1,500 DiD-stained myHSCs and lyHSCs were suspended in approximately 100 µl of Ca^{2+}/Mg^{2+}-free D-PBS and adoptively transferred via retro-orbital injection into anesthetized young WT and Sema4AKO mice. One day before transplantation, recipient mice were lethally irradiated (1,200 cGy) using an X-ray irradiator (Precision, X-Rad320) with a split dose of 600 cGy + 600 cGy with a 3-h interval between doses.

For intravital imaging, mice were prepared as previously described[85]. In brief, 14–15 h after transplantation, the mice were anaesthetized with an induction dose of 3–4% isoflurane and a maintenance dose of 1.5–2% isoflurane. Z-stacks were acquired with 2-µm steps at 10-min intervals for 90 min in 4–8 fields of view. Transplanted cells were classified as single or cluster cells when the nearest cell-to-cell edge distance was more than 15 µm or less than 15 µm, respectively.

Cell preparation for bulk RNA-seq. For myHSC/lyHSC profiling, 100 cells from each fraction of interest were sorted into the lysis buffer (10% Triton X-100 (Sigma-Aldrich) and SUPERase-In RNase Inhibitor 20 U $µl^{-1}$ (Ambion)) and snap frozen. cDNA amplification was performed as per Smart-Seq2 protocol. Fragmentation and sample barcoding were performed using a NEBNext Ultra II FS DNA Library Prep Kit for Illumina (New England Biolabs) according to the manufacturer's guidelines. Samples were sequenced on a 200-cycle NovaSeq SP.

Cell preparation for single-cell RNA-seq. *HSPCs*. BMMNCs were stained with conjugated monoclonal antibodies for HSPC markers as described above. Then, 10,000 Lin^-Kit^+ cells from young or aged WT/Sema4AKO mice were sorted in Ca^{2+}/Mg^{2+}-free D-PBS supplemented with 2% BSA (New England Biolabs). After one round of centrifugation, the cells were processed on a 10x Genomics platform according to the manufacturer's protocol.

myHSCs/lyHSCs. BMMNCs were stained with conjugated monoclonal antibodies for HSPC markers as described above except for CD34 to minimize staining time and prevent RNA degradation (CD34 staining requires 90 min[86]). myHSCs and lyHSCs were sorted into 96-well plates with the lysis buffer and stored frozen at −80 °C. cDNA amplification and sequencing were performed as per Smart-Seq2 protocol[87].

Bulk sequencing analysis. RNA-seq reads were aligned and counted using STAR[88] with the GRCm39 mouse genome assembly and Ensembl 106 (ref. 89) gene annotations. Differential expression was called using DESeq2 (ref. 90). Genes were considered differentially expressed if their *q* values (that is, FDR-adjusted *P* value) were less than 0.05. GSEA was performed on the Molecular Signatures Database (MSigDB) mouse hallmark gene set[91]. For this analysis, genes were ranked by the Z-test statistic calculated by DESeq2, where more extreme negative or positive values correspond to more significantly downregulated or upregulated genes, respectively. The ranked lists of genes were tested using the GSEAPreranked test[92] accessed through the GSEApy interface[93]. Significant gene sets were those with a *q* value less than 0.01.

Single-cell RNA-seq sample processing and data analysis

10x Genomics. *Library preparation*. Libraries from 10,000 Kit^+ cells each from WT ($n = 1$) and Sema4A KO ($n = 2$) young and WT ($n = 2$) old mice were prepared using the Single Cell 3′ Reagent Kit v3 (10x Genomics) according to the manufacturer's protocol.

Quality control and data normalization. The Cell Ranger 3.1.0 (10x Genomics) analysis pipeline was used to process the 10x single-cell RNA-seq output by aligning reads to mm10-3.0.0 mouse transcriptome (Ensembl). Cell Ranger was also used to aggregate condition replicates before processing. For all the analysis steps specified below, we used the SCANPY library[94], unless specified otherwise. As a quality control, first we filtered out cells with fewer than 200 genes detected with more than zero reads, and we removed genes present in fewer than three cells. We also removed cells with a high percentage of reads mapped to mitochondrial genes (>5%) and a high number of detected genes (>6,500). With the tool Scrublet[95], we predicted and removed doublets from the dataset.

After concatenating the data from WT and Sema4AKO mice, we normalized the data for sequencing depth to a target of 1×10^4 counts per cell. Then, after adding 1 as pseudocount, the count matrix was log transformed. Finally, the total counts per cell as well as the percentage of reads mapping to mitochondrial genes were regressed out.

Data clustering and visualization. We identified highly variable genes with the SCANPY function 'sc.pp.highly_variable_genes' (parameters: min_mean = 0.0125, max_mean = 3, min_disp = 0.5), and we computed a neighborhood graph (n_neighbors = 8) on the first 40 PCs. To visualize the data, the graph was embedded in two dimensions using uniform manifold approximation and projection (UMAP)[96].

We clustered the neighborhood graph using the Leiden clustering algorithm[97] with resolution 1 and 0.3 for young and old mice, respectively. This resulted in 28 clusters in the young mice dataset and 17 clusters in the old mice dataset. The WT and Sema4AKO young dataset was subsetted to exclude small, isolated clusters and re-clustered with resolution 0.2. Cluster marker genes were found with a Wilcoxon rank-sum test. Based on known HSC markers (Ly6a, Procr and Hoxb5), we identified the cluster corresponding to HSCs in the dataset from WT and Sema4AKO young mice (cluster 1), which was used for the enrichment analysis. In the WT old mice dataset, we similarly identified HSCs and early MPPs using marker genes and by predicted lineage relationships using graph abstraction[42], and, based on them, we built a differentiation trajectory for DPT analysis (see above).

Differential gene expression and enrichment analysis. We identified the genes differentially expressed between the WT and Sema4AKO cells in the HSC cluster 1 from young mice using a Wilcoxon test. For the pathway enrichment analysis, the top 500 upregulated and downregulated genes were ranked by statistical significance, and the GSEA tool from the Broad Institute was used to perform enrichment analysis as described for bulk sequencing[98].

Smart-Seq2 data analysis. *Raw data processing and normalization*. We quantified the abundance of the transcripts from 768 cells with Salmon (version 0.17)[99]. First, we indexed the mouse transcriptome (GRCm38) in quasi-mapping-based mode with –seqBias and –gcBias flags. Then, we aggregated the transcript-level abundances into gene-level abundances, which, in turn, were transformed into a gene–cell count matrix. Next, quality control was performed to filter out cells that satisfy any of the following criteria: (1) fewer than 4,000 genes detected (detection threshold: reads per million > 10); (2) overall mapping less than 50%; (3) fraction of reads mapping to mitochondrial transcripts greater than 0.02; and (4) fraction of reads mapping to ERCC spike-ins greater than 0.01. After quality control, we retained 642 cells for downstream analyses (155 WT myHSCs, 157 WT lyHSCs, 166 KO myHSCs and 164 KO lyHSCs). The data were normalized using 'quickcluster' and 'computeSumFactors' functions from the scran package in R[100]. Finally, we added a pseudocount of 1 to the count matrix, followed by natural log transformation.

Batch integration and visualization. Because the data were collected from two separate batches, we performed batch integration before visualizing the data. For this purpose, we used the Seurat batch integration

workflow[101]. First, 3,000 highly variable genes were selected from each batch. Then, we used the FindIntegrationAnchors function to estimate the anchors to use for the integration with 3,000 features (anchor.features = 3,000) and the first 20 canonical variates (dims = 1:20). Finally, the 'IntegrateData' function was used with default parameters to integrate the two batches.

To visualize the cells on a low-dimensional space, we first built a *k*-nearest neighbor graph with the 'neighbors' function from SCANPY[93] with 10 PCs and $k = 30$. Then, the 'tl.umap' function was used to calculate a UMAP representation[102], and the first two UMAP components were plotted. We applied this procedure separately for myHSCs and lyHSCs. To verify if myHSCs and lyHSCs are differentially affected by the absence of Sema4A, we calculated the pairwise Spearman's correlation distance (defined as $(1-\rho)2$, where ρ is the Spearman's correlation coefficient computed on the top 3,000 highly variable genes identified with Seurat) between WT and KO cells for myHSCs and lyHSCs separately. Then, we tested the statistical significance of the difference between the two distributions of pairwise distances by using the Wilcoxon rank-sum test.

DPT analysis. For this analysis, we first generated 10x Genomics single-cell RNA-seq profiles of $Lin^{-}c\text{-}Kit^{+}$ HSPCs from 74-week-old WT animals—that is, age matched with WT/Sema4AKO animals for the Smart-Seq2 single-cell RNA-seq experiment described above. In this 10x dataset, we used previously described markers to map the clusters corresponding to HSC (*Ly6a*, *Procr* and *Hlf*) and MPP (*Cd34*, *Cebpa* and *Ctsg*)[103] and used the transcriptomes of cells within these clusters to estimate a differentiation trajectory, in which higher DPT values correspond to more mature cells (data not shown). For this purpose, a *k*-nearest neighbor graph was first built with the first five PCs and $k = 15$. A diffusion map was then constructed with the 'tl.diffmap' function from SCANPY. We defined a DPT by selecting the root cell that had the lowest value of the first diffusion component[42]. As expected, analysis of known self-renewing marker genes revealed downregulation of vWF, *Mpl*, *Fdg5*, *Ctnnal1* and *Procr* and upregulation of *Ctsg* and *Cbpa* as cells progressed from HSC to MPP (Supplementary Note 2). Finally, we used these differentiation trajectories to test the difference in the distribution of DPT values for both WT and KO myHSCs, which we estimated with the Wilcoxon rank-sum test.

Differential gene expression analysis. We found DEGs between KO and WT with the DEseq2 package[90] on R. First, we removed genes that were expressed in fewer than 10 cells for each batch, and the counts were rounded to integers. Then, we created a DESeq object from the count matrix with the design ~condition+batch. Fold changes (FCs) and *P* values were estimated using the DESeq function with default parameters.

ATAC-seq analysis. All sequencing reads were trimmed using Cutadapt[104], and trimmed reads (>36-bp minimum alignment length) were mapped against the mm10 genome using BWA aligner[105]. We used de-duplicated and uniquely mapped reads for peak calling analysis after excluding high-sensitive blacklist regions defined by ENCODE. The candidate peaks were predicted by MACS peak calling software (FDR < 0.05)[106]. After identifying narrow peaks from biological replicates, we created a merged set of consensus peaks and generated a matrix of OCRs. Then, we calculated the number of mapped reads located at the center of the peaks (±250 bp from mid-point). This OCR matrix was then imported into the R package DESeq2 (ref. 90), and we determined differentially accessible regions (DARs) with the following cutoffs: (1) FC > 1.5, counts per million (CPM) > 1.0, *P* value (stringent cutoffs); (2) FC > 1.2, CPM > 1.0, $P < 0.01$ (relaxed cutoffs). We identified 2,379 gain of accessible peaks (enriched in MUL) and 2,028 loss of accessible peaks (enriched in PLT) for the Nerlov group's ATAC-seq datasets (stringent cutoff). We also identified 215 gain of accessible peaks (enriched in Sema4aKO) and 112 loss of accessible peaks (enriched in WT) from our myHSC ATAC-seq datasets (relaxed cutoffs). Finally, the candidate differential OCRs were submitted to search for potential transcription factor binding sites using HOMER software[107] with all open chromatin peaks as background regions. In this analysis, de novo motif (unbiased way to find motifs using various k-mers) and known motif searches using HOMER known motif database were performed, and we reported the top de novo motif or known motif results. CREB5 and RUNX3 motifs were identified from both de novo and known motif analysis in Sema4AKO-enriched DARs. RUNX3 was the second highest motif from known motifs.

Statistics and reproducibility. The number of mice chosen for each experiment is based on the principle that minimal number of mice is used to have statistical power and is similar to published literature for the same assays performed[24]. Data points were excluded if they were identified as outliers using Grubbs' test. No randomization method was used to allocate mice to experimental groups. The mice from the different groups were mixed together to exclude cage effects as a covariate. Because observer bias is not relevant for most of the in vivo experiments, no blinding was used during data collection. However, in the experiments involving image analysis (histology and intravital imaging), where observer bias may have been a concern, the investigators were blinded to the genetic background of the animals. Measurements were taken from distinct samples from different mice. Statistical analysis was performed with Student's *t*-tests (in Excel), unless specified otherwise. Data distribution was assumed to be normal, but this was not formally tested. Data are presented as the mean, and the error bars represent the s.e.m. In all corresponding figures, $^{*}P < 0.05$, $^{**}P < 0.01$, $^{***}P < 0.001$ and not significant (NS) $P > 0.05$. Information about replication is indicated in the figures and figure legends.

Reporting summary

Further information on research design is available in the Nature Portfolio Reporting Summary linked to this article.

Data availability

All data supporting the findings of the study are available from the corresponding author. All data were analyzed with standard programs and packages, as detailed in the Methods. RNA-seq data from this study are available from ArrayExpress (E-MTAB-11359 (single-cell RNA-seq of aged WT/Sema4AKO myHSCs and lyHSCs) and E-MTAB-12890 (bulk RNA-seq of WT/Sema4AKO myHSCs/lyHSCs at baseline and after acute LPS)). ATAC-seq data from this study are available from the Gene Expression Omnibus (GSE281145).

References

1. Scaramozza, A. et al. Lineage tracing reveals a subset of reserve muscle stem cells capable of clonal expansion under stress. *Cell Stem Cell* **24**, 944–957 (2019).
2. Ibrayeva, A. et al. Early stem cell aging in the mature brain. *Cell Stem Cell* **28**, 955–966 (2021).
3. Altshuler, A. et al. Discrete limbal epithelial stem cell populations mediate corneal homeostasis and wound healing. *Cell Stem Cell* **28**, 1248–1261 (2021).
4. Farrelly, O. et al. Two-photon live imaging of single corneal stem cells reveals compartmentalized organization of the limbal niche. *Cell Stem Cell* **28**, 1233–1247 (2021).
5. Hsu, Y. C., Pasolli, H. A. & Fuchs, E. Dynamics between stem cells, niche, and progeny in the hair follicle. *Cell* **144**, 92–105 (2011).
6. Matatall, K. A., Shen, C. C., Challen, G. A. & King, K. Y. Type II interferon promotes differentiation of myeloid-biased hematopoietic stem cells. *Stem Cells* **32**, 3023–3030 (2014).
7. Yamamoto, R., Wilkinson, A. C. & Nakauchi, H. Changing concepts in hematopoietic stem cells. *Science* **362**, 895–896 (2018).

8. Yamamoto, R. et al. Clonal analysis unveils self-renewing lineage-restricted progenitors generated directly from hematopoietic stem cells. *Cell* **154**, 1112–1126 (2013).
9. Florez, M. A. et al. Interferon gamma mediates hematopoietic stem cell activation and niche relocalization through BST2. *Cell Rep.* **33**, 108530 (2020).
10. Beerman, I. et al. Functionally distinct hematopoietic stem cells modulate hematopoietic lineage potential during aging by a mechanism of clonal expansion. *Proc. Natl Acad. Sci. USA* **107**, 5465–5470 (2010).
11. Challen, G. A., Boles, N. C., Chambers, S. M. & Goodell, M. A. Distinct hematopoietic stem cell subtypes are differentially regulated by TGF-β1. *Cell Stem Cell* **6**, 265–278 (2010).
12. Sanjuan-Pla, A. et al. Platelet-biased stem cells reside at the apex of the haematopoietic stem-cell hierarchy. *Nature* **502**, 232–236 (2013).
13. Carrelha, J. et al. Hierarchically related lineage-restricted fates of multipotent haematopoietic stem cells. *Nature* **554**, 106–111 (2018).
14. Notta, F. et al. Distinct routes of lineage development reshape the human blood hierarchy across ontogeny. *Science* **351**, aab2116 (2016).
15. Pang, W. W. et al. Human bone marrow hematopoietic stem cells are increased in frequency and myeloid-biased with age. *Proc. Natl Acad. Sci. USA* **108**, 20012–20017 (2011).
16. Mitroulis, I. et al. Modulation of myelopoiesis progenitors is an integral component of trained immunity. *Cell* **172**, 147–161 (2018).
17. Bogeska, R. et al. Inflammatory exposure drives long-lived impairment of hematopoietic stem cell self-renewal activity and accelerated aging. *Cell Stem Cell* **29**, 1273–1284 (2022).
18. Goodell, M. A. & Rando, T. A. Stem cells and healthy aging. *Science* **350**, 1199–1204 (2015).
19. Mann, M. et al. Heterogeneous responses of hematopoietic stem cells to inflammatory stimuli are altered with age. *Cell Rep.* **25**, 2992–3005 (2018).
20. Alto, L. T. & Terman, J. R. Semaphorins and their signaling mechanisms. *Methods Mol. Biol.* **1493**, 1–25 (2017).
21. Kumanogoh, A. et al. Class IV semaphorin Sema4A enhances T-cell activation and interacts with Tim-2. *Nature* **419**, 629–633 (2002).
22. Kumanogoh, A. et al. Nonredundant roles of Sema4A in the immune system: defective T cell priming and Th1/Th2 regulation in Sema4A-deficient mice. *Immunity* **22**, 305–316 (2005).
23. Toyofuku, T. et al. Semaphorin-4A, an activator for T-cell-mediated immunity, suppresses angiogenesis via Plexin-D1. *EMBO J.* **26**, 1373–1384 (2007).
24. Silberstein, L. et al. Proximity-based differential single-cell analysis of the niche to identify stem/progenitor cell regulators. *Cell Stem Cell* **19**, 530–543 (2016).
25. Goncalves, K. A. et al. Angiogenin promotes hematopoietic regeneration by dichotomously regulating quiescence of stem and progenitor cells. *Cell* **166**, 894–906 (2016).
26. Takamatsu, H. & Kumanogoh, A. Diverse roles for semaphorin–plexin signaling in the immune system. *Trends Immunol.* **33**, 127–135 (2012).
27. Delgoffe, G. M. et al. Stability and function of regulatory T cells is maintained by a neuropilin-1–semaphorin-4a axis. *Nature* **501**, 252–256 (2013).
28. Haematolymphoid Tumours. *WHO Classification of Tumours* 5th edn (World Health Organization, 2024).
29. Ho, Y. H. et al. Remodeling of bone marrow hematopoietic stem cell niches promotes myeloid cell expansion during premature or physiological aging. *Cell Stem Cell* **25**, 407–418 (2019).
30. Pronk, C. J. et al. Elucidation of the phenotypic, functional, and molecular topography of a myeloerythroid progenitor cell hierarchy. *Cell Stem Cell* **1**, 428–442 (2007).
31. Liang, Y., Van Zant, G. & Szilvassy, S. J. Effects of aging on the homing and engraftment of murine hematopoietic stem and progenitor cells. *Blood* **106**, 1479–1487 (2005).
32. Karakaslar, E. O. et al. Transcriptional activation of Jun and Fos members of the AP-1 complex is a conserved signature of immune aging that contributes to inflammaging. *Aging Cell* **22**, e13792 (2023).
33. Trizzino, M. et al. EGR1 is a gatekeeper of inflammatory enhancers in human macrophages. *Sci. Adv.* **7**, eaaz8836 (2021).
34. Jia, D. et al. Cardiac resident macrophage-derived legumain improves cardiac repair by promoting clearance and degradation of apoptotic cardiomyocytes after myocardial infarction. *Circulation* **145**, 1542–1556 (2022).
35. Marzio, R., Jirillo, E., Ransijn, A., Mauel, J. & Corradin, S. B. Expression and function of the early activation antigen CD69 in murine macrophages. *J. Leukoc. Biol.* **62**, 349–355 (1997).
36. Konturek-Ciesla, A., Olofzon, R., Kharazi, S. & Bryder, D. Implications of stress-induced gene expression for hematopoietic stem cell aging studies. *Nat. Aging* **4**, 177–184 (2024).
37. Yoshida, H. et al. The *cis*-regulatory atlas of the mouse immune system. *Cell* **176**, 897–912 (2019).
38. King, K. Y. et al. Irgm1 protects hematopoietic stem cells by negative regulation of IFN signaling. *Blood* **118**, 1525–1533 (2011).
39. Weih, F. et al. Multiorgan inflammation and hematopoietic abnormalities in mice with a targeted disruption of RelB, a member of the NF-κ B/Rel family. *Cell* **80**, 331–340 (1995).
40. Li, J. et al. STAT1 is essential for HSC function and maintains MHCII^{hi} stem cells that resist myeloablation and neoplastic expansion. *Blood* **140**, 1592–1606 (2022).
41. Becker-Herman, S. et al. CD74 is a regulator of hematopoietic stem cell maintenance. *PLoS Biol.* **19**, e3001121 (2021).
42. Haghverdi, L., Buttner, M., Wolf, F. A., Buettner, F. & Theis, F. J. Diffusion pseudotime robustly reconstructs lineage branching. *Nat. Methods* **13**, 845–848 (2016).
43. Kovtonyuk, L. V., Fritsch, K., Feng, X., Manz, M. G. & Takizawa, H. Inflamm-aging of hematopoiesis, hematopoietic stem cells, and the bone marrow microenvironment. *Front. Immunol.* **7**, 502 (2016).
44. Flohr Svendsen, A. et al. A comprehensive transcriptome signature of murine hematopoietic stem cell aging. *Blood* **138**, 439–451 (2021).
45. Wilson, N. K. et al. Combined single-cell functional and gene expression analysis resolves heterogeneity within stem cell populations. *Cell Stem Cell* **16**, 712–724 (2015).
46. Cabezas-Wallscheid, N. et al. Identification of regulatory networks in HSCs and their immediate progeny via integrated proteome, transcriptome, and DNA methylome analysis. *Cell Stem Cell* **15**, 507–522 (2014).
47. Laurenti, E. et al. CDK6 levels regulate quiescence exit in human hematopoietic stem cells. *Cell Stem Cell* **16**, 302–313 (2015).
48. Fernando, R. N. et al. Cell cycle restriction by histone H2AX limits proliferation of adult neural stem cells. *Proc. Natl Acad. Sci. USA* **108**, 5837–5842 (2011).
49. Qian, H. et al. Critical role of thrombopoietin in maintaining adult quiescent hematopoietic stem cells. *Cell Stem Cell* **1**, 671–684 (2007).
50. Pietras, E. M. et al. Functionally distinct subsets of lineage-biased multipotent progenitors control blood production in normal and regenerative conditions. *Cell Stem Cell* **17**, 35–46 (2015).
51. Adolfsson, J. et al. Identification of Flt3^{+} lympho-myeloid stem cells lacking erythro-megakaryocytic potential a revised road map for adult blood lineage commitment. *Cell* **121**, 295–306 (2005).

52. Chen, X. et al. Bone marrow myeloid cells regulate myeloid-biased hematopoietic stem cells via a histamine-dependent feedback loop. *Cell Stem Cell* **21**, 747–760 (2017).
53. Esplin, B. L. et al. Chronic exposure to a TLR ligand injures hematopoietic stem cells. *J. Immunol.* **186**, 5367–5375 (2011).
54. Demel, U. M. et al. A complex proinflammatory cascade mediates the activation of HSCs upon LPS exposure in vivo. *Blood Adv.* **6**, 3513–3528 (2022).
55. Walter, D. et al. Exit from dormancy provokes DNA-damage-induced attrition in haematopoietic stem cells. *Nature* **520**, 549–552 (2015).
56. Komorowska, K. et al. Hepatic leukemia factor maintains quiescence of hematopoietic stem cells and protects the stem cell pool during regeneration. *Cell Rep.* **21**, 3514–3523 (2017).
57. Warr, M. R. et al. FOXO3A directs a protective autophagy program in haematopoietic stem cells. *Nature* **494**, 323–327 (2013).
58. Passegué, E., Wagers, A. J., Giuriato, S., Anderson, W. C. & Weissman, I. L. Global analysis of proliferation and cell cycle gene expression in the regulation of hematopoietic stem and progenitor cell fates. *J. Exp. Med.* **202**, 1599–1611 (2005).
59. Cabezas-Wallscheid, N. et al. Vitamin A-retinoic acid signaling regulates hematopoietic stem cell dormancy. *Cell* **169**, 807–823 (2017).
60. Yu, W. et al. Plexin-B2 mediates physiologic and pathologic functions of angiogenin. *Cell* **171**, 849–864 (2017).
61. Kwok, A. J. et al. Neutrophils and emergency granulopoiesis drive immune suppression and an extreme response endotype during sepsis. *Nat. Immunol.* **24**, 767–779 (2023).
62. Zhang, Y. et al. *Tie2Cre*-mediated inactivation of plexinD1 results in congenital heart, vascular and skeletal defects. *Dev. Biol.* **325**, 82–93 (2009).
63. Ding, J. B., Oh, W. J., Sabatini, B. L. & Gu, C. Semaphorin 3E–Plexin-D1 signaling controls pathway-specific synapse formation in the striatum. *Nat. Neurosci.* **15**, 215–223 (2011).
64. Kim, M. H. et al. A late-lineage murine neutrophil precursor population exhibits dynamic changes during demand-adapted granulopoiesis. *Sci. Rep.* **7**, 39804 (2017).
65. Passegue, E., Wagner, E. F. & Weissman, I. L. JunB deficiency leads to a myeloproliferative disorder arising from hematopoietic stem cells. *Cell* **119**, 431–443 (2004).
66. Abram, C. L., Roberge, G. L., Hu, Y. & Lowell, C. A. Comparative analysis of the efficiency and specificity of myeloid-Cre deleting strains using ROSA-EYFP reporter mice. *J. Immunol. Methods* **408**, 89–100 (2014).
67. Dykstra, B. et al. Long-term propagation of distinct hematopoietic differentiation programs in vivo. *Cell Stem Cell* **1**, 218–229 (2007).
68. Meng, Y. et al. Epigenetic programming defines haematopoietic stem cell fate restriction. *Nat. Cell Biol.* **25**, 812–822 (2023).
69. Lee, J. W. et al. RUNX3 regulates cell cycle-dependent chromatin dynamics by functioning as a pioneer factor of the restriction-point. *Nat. Commun.* **10**, 1897 (2019).
70. Pinho, S. et al. Lineage-biased hematopoietic stem cells are regulated by distinct niches. *Dev. Cell* **44**, 634–641 (2018).
71. Morita, Y., Ema, H. & Nakauchi, H. Heterogeneity and hierarchy within the most primitive hematopoietic stem cell compartment. *J. Exp. Med.* **207**, 1173–1182 (2010).
72. Luchsinger, L. L., de Almeida, M. J., Corrigan, D. J., Mumau, M. & Snoeck, H. W. Mitofusin 2 maintains haematopoietic stem cells with extensive lymphoid potential. *Nature* **529**, 528–531 (2016).
73. Song, Z. et al. An NAD^+-dependent metabolic checkpoint regulates hematopoietic stem cell activation and aging. *Nat. Aging* **4**, 1384–1393 (2024).
74. Kwak, H. J. et al. Myeloid cell-derived reactive oxygen species externally regulate the proliferation of myeloid progenitors in emergency granulopoiesis. *Immunity* **42**, 159–171 (2015).
75. Zhu, H. et al. Reactive oxygen species-producing myeloid cells act as a bone marrow niche for sterile inflammation-induced reactive granulopoiesis. *J. Immunol.* **198**, 2854–2864 (2017).
76. Wang, L. et al. Expression of Semaphorin 4A and its potential role in rheumatoid arthritis. *Arthritis Res. Ther.* **17**, 227 (2015).
77. Young, K. et al. Decline in IGF1 in the bone marrow microenvironment initiates hematopoietic stem cell aging. *Cell Stem Cell* **28**, 1473–1482 (2021).
78. Arthur, L. et al. Cellular and plasma proteomic determinants of COVID-19 and non-COVID-19 pulmonary diseases relative to healthy aging. *Nat. Aging* **1**, 535–549 (2021).
79. Choi, Y. I. et al. PlexinD1 glycoprotein controls migration of positively selected thymocytes into the medulla. *Immunity* **29**, 888–898 (2008).
80. Dai, X. et al. A novel role for myeloid cell-specific neuropilin 1 in mitigating sepsis. *FASEB J.* **31**, 2881–2892 (2017).
81. Zeng, A. G. X. et al. Identification of a human hematopoietic stem cell subset that retains memory of inflammatory stress. Preprint at *bioRxiv* https://doi.org/10.1101/2023.09.11.557271 (2023).
82. Xia, J. et al. Semaphorin-plexin signaling controls mitotic spindle orientation during epithelial morphogenesis and repair. *Dev. Cell* **33**, 299–313 (2015).
83. Galvin, A. et al. Cell cycle analysis of hematopoietic stem and progenitor cells by multicolor flow cytometry. *Curr. Protoc. Cytom.* **87**, e50 (2019).
84. Feng, C. G., Weksberg, D. C., Taylor, G. A., Sher, A. & Goodell, M. A. The p47 GTPase Lrg-47 (Irgm1) links host defense and hematopoietic stem cell proliferation. *Cell Stem Cell* **2**, 83–89 (2008).
85. Christodoulou, C. et al. Live-animal imaging of native haematopoietic stem and progenitor cells. *Nature* **578**, 278–283 (2020).
86. Ema, H. et al. Adult mouse hematopoietic stem cells: purification and single-cell assays. *Nat. Protoc.* **1**, 2979–2987 (2006).
87. Picelli, S. et al. Full-length RNA-seq from single cells using Smart-seq2. *Nat. Protoc.* **9**, 171–181 (2014).
88. Dobin, A. et al. STAR: ultrafast universal RNA-seq aligner. *Bioinformatics* **29**, 15–21 (2013).
89. Cunningham, F. et al. Ensembl 2022. *Nucleic Acids Res.* **50**, D988–D995 (2022).
90. Love, M. I., Huber, W. & Anders, S. Moderated estimation of fold change and dispersion for RNA-seq data with DESeq2. *Genome Biol.* **15**, 550 (2014).
91. Liberzon, A. et al. The Molecular Signatures Database (MSigDB) hallmark gene set collection. *Cell Syst.* **1**, 417–425 (2015).
92. Reimand, J. et al. Pathway enrichment analysis and visualization of omics data using g:Profiler, GSEA, Cytoscape and EnrichmentMap. *Nat. Protoc.* **14**, 482–517 (2019).
93. Fang, Z., Liu, X. & Peltz, G. GSEApy: a comprehensive package for performing gene set enrichment analysis in Python. *Bioinformatics* **39**, btac757 (2023).
94. Wolf, F. A., Angerer, P. & Theis, F. J. SCANPY: large-scale single-cell gene expression data analysis. *Genome Biol.* **19**, 15 (2018).
95. Wolock, S. L., Lopez, R. & Klein, A. M. Scrublet: computational identification of cell doublets in single-cell transcriptomic data. *Cell Syst.* **8**, 281–291 (2019).
96. McInnes, L., Healy, J. & Melville, J. UMAP: uniform manifold approximation and projection for dimension reduction. Preprint at *arXiv* https://doi.org/10.48550/arXiv.1802.03426 (2020).
97. Traag, V. A., Waltman, L. & van Eck, N. J. From Louvain to Leiden: guaranteeing well-connected communities. *Sci. Rep.* **9**, 5233 (2019).
98. Subramanian, A. et al. Gene set enrichment analysis: a knowledge-based approach for interpreting genome-wide expression profiles. *Proc. Natl Acad. Sci. USA* **102**, 15545–15550 (2005).

99. Patro, R., Duggal, G., Love, M. I., Irizarry, R. A. & Kingsford, C. Salmon provides fast and bias-aware quantification of transcript expression. *Nat. Methods* **14**, 417–419 (2017).
100. Lun, A. T., Bach, K. & Marioni, J. C. Pooling across cells to normalize single-cell RNA sequencing data with many zero counts. *Genome Biol.* **17**, 75 (2016).
101. Butler, A., Hoffman, P., Smibert, P., Papalexi, E. & Satija, R. Integrating single-cell transcriptomic data across different conditions, technologies, and species. *Nat. Biotechnol.* **36**, 411–420 (2018).
102. Becht, E. et al. Dimensionality reduction for visualizing single-cell data using UMAP. *Nat. Biotechnol.* https://doi.org/10.1038/nbt.4314 (2018).
103. Nestorowa, S. et al. A single-cell resolution map of mouse hematopoietic stem and progenitor cell differentiation. *Blood* **128**, e20–e31 (2016).
104. Martin, M. Cutadapt removes adapter sequences from high-throughput sequencing reads. *EMBnet J.* https://doi.org/10.14806/ej.17.1.200 (2011).
105. Li, H. & Durbin, R. Fast and accurate short read alignment with Burrows–Wheeler transform. *Bioinformatics* **25**, 1754–1760 (2009).
106. Zhang, Y. et al. Model-based analysis of ChIP-Seq (MACS). *Genome Biol.* **9**, R137 (2008).
107. Heinz, S. et al. Simple combinations of lineage-determining transcription factors prime *cis*-regulatory elements required for macrophage and B cell identities. *Mol. Cell* **38**, 576–589 (2010).

Acknowledgements

The authors would like to acknowledge the Core Facilities of Fred Hutchinson Cancer Center; E. Regiarto, M. Baum and K. Krum for technical help; and A. Wilkinson and S. Mckinney-Freeman for helpful discussions and critical reading of the manuscript. This study was supported by National Institutes of Health grant RO1 HL148189, the New Development Fund from the Fred Hutchinson Cancer Center and Leukemia and Lymphoma Society Translational Research Program award to L.S. E.M.P. is a Scholar of the Leukemia and Lymphoma Society.

Author contributions

L.S. conceived the study. D.T., S.G., S.Z., S. Radtke, H.-P.K., S. Rodriguez, N.C., A.P., A.G., E.M.P. and D.T.S. characterized mutant mouse strains. N.S., C.B., D.G. and J.A.S. performed intravital microscopy experiments. E.M., E.I.C., N.K.W., S.J.K., B.G., P.K., D.J., A.T. and A.S. generated and analyzed bulk and single-cell RNA-seq data. L.Z., I.B., B.P. and D.H.J. generated and analyzed ATAC-seq data. A.K. provided the Sema4AKO mice; T.W. provided the Sema4A-floxed mice; and C.N. provided the vWF-Tomato mice. M.M., C.M. and F.L. performed the bone histology analysis. J.-G.C. and S.Z.J. provided human HSC gene expression data. L.S. wrote the manuscript, with contributions from all authors.

Competing interests

L.S., S. Radtke and H.P.-K. are listed inventors on patent application 18/717,971 relating to this work. All other authors declare no competing interests.

Additional information

Extended data is available for this paper at https://doi.org/10.1038/s43587-024-00798-7.

Supplementary information The online version contains supplementary material available at https://doi.org/10.1038/s43587-024-00798-7.

Correspondence and requests for materials should be addressed to Lev Silberstein.

Peer review information *Nature Aging* thanks Yu Hou and the other, anonymous, reviewer(s) for their contribution to the peer review of this work.

Reprints and permissions information is available at www.nature.com/reprints.

Publisher's note Springer Nature remains neutral with regard to jurisdictional claims in published maps and institutional affiliations.

[1]Translational Science and Therapeutics Division, Fred Hutchinson Cancer Research Center, Seattle, WA, USA. [2]Institute of Epigenetics and Stem Cells (IES), Helmholtz Zentrum Muenchen, Munich, Germany. [3]Department of Bioengineering, University of California, Merced, Merced, CA, USA. [4]Department of Stem Cell Biology & Regenerative Medicine, Beckman Research Institute of City of Hope, Duarte, CA, USA. [5]Department of Haematology, Jeffrey Cheah Biomedical Centre, Wellcome - MRC Cambridge Stem Cell Institute, University of Cambridge, Cambridge, UK. [6]Epigenetics and Stem Cell Aging Unit, National Institute of Aging, Baltimore, MD, USA. [7]Department of Epigenetics, Van Del Institute, Grand Rapids, MI, USA. [8]Radcliffe Department of Medicine, University of Oxford, Oxford, UK. [9]Department of Medicine-Hematology, University of Colorado School of Medicine, Aurora, CO, USA. [10]Department of Development and Regeneration, KU Leuven, Leuven, Belgium. [11]Department of Respiratory Medicine, Allergy and Rheumatic Diseases, University of Osaka, Osaka, Japan. [12]Faculty of Medicine, Institute of Pharmacology, University of Marburg, Marburg, Germany. [13]Department of Pathology and Laboratory Medicine, Weill Cornell Medicine, New York, NY, USA. [14]Immunology and Microbial Pathogenesis Program, Weill Cornell Medicine, New York, NY, USA. [15]Department of Stem Cell and Regenerative Biology, Harvard University, Boston, MA, USA. [16]These authors contributed equally: Dorsa Toghani, Sanika Gupte. ✉e-mail: lsilbers@fredhutch.org

https://doi.org/10.1038/s43587-024-00798-7

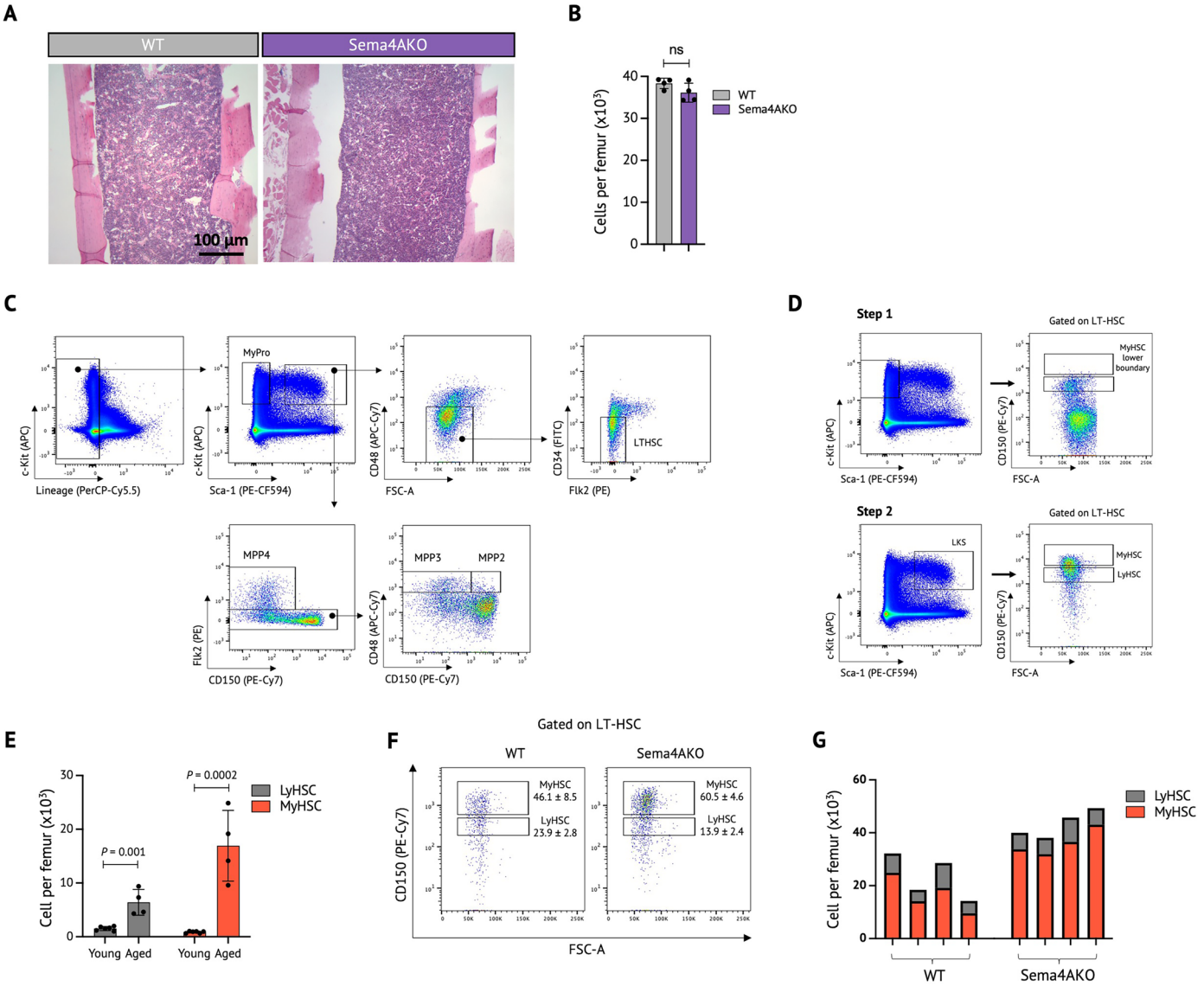

Extended Data Fig. 1 | The absence of Sema4A leads to excessive myeloid expansion and premature hematopoietic aging-like phenotype. **A**. Representative images of H&E staining of femurs from aged WT/Sema4AKO mice (n = 4 mice per group). **B**. Bone marrow cellularity of aged WT/Sema4AKO mice (n = 4 mice per group). **C**. Gating strategy for flow cytometric analysis of primitive bone marrow subsets (WT aged mice are shown). LT-HSC denotes long-term HSC. **D**. Gating strategy for flow cytometric identification of myHSC and lyHSC based on intensity of CD150 expression. **E**. Absolute numbers of myHSC and lyHSC in young and aged WT mice (n = 6 mice for young group and n = 4 mice for aged group) **F**. Representative plots of myHSC quantification in aged WT/Sema4KO mice. **G**. Absolute number of myHSC and lyHSC in individual aged WT/Sema4AKO mice. P values are shown. Statistical significance was assessed by two-tailed t-test. Mean +/- (SEM) are shown.

https://doi.org/10.1038/s43587-024-00798-7

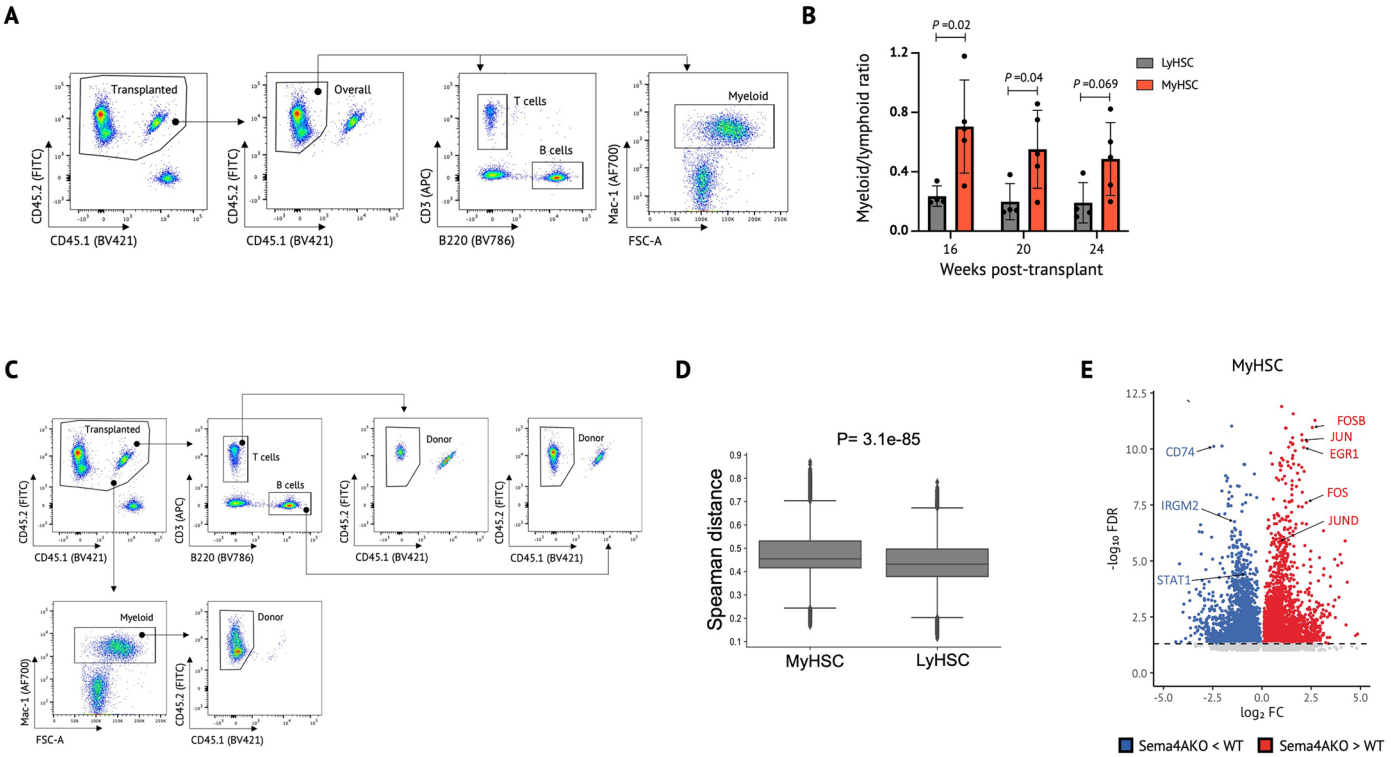

Extended Data Fig. 2 | The absence of Sema4A leads to functional attrition of myHSC during aging. A. Gating strategy for quantification of overall reconstitution by donor-derived HSC and analysis of lineage composition of donor-derived graft. **B**. Myeloid/lymphoid ratio of peripheral blood donor-derived cells (CD45.2) in WT mice (CD45.1) which were competitively transplanted with aged WT myHSC or aged WT lyHSC (CD45.2) (n = 5 animals per group). **C**. Gating strategy for quantification of lineage contribution by donor-derived cells. **D**. Distribution of pairwise Spearman's correlation distances between aged WT and Sema4AKO myHSC (left) and lyHSC (right) (n = 642 cells across 2 biological replicates and 4 technical replicates). In box plot, centre line shows median, box limits indicate upper and lower quartiles, whiskers extend to minimum and maximum values **E**. Volcano plots showing DEGs in myHSC from aged WT and Sema4AKO mice. The x and y axes indicate the expression fold change (FC) (log2) and the false discovery rate (FDR) (− log10) for each gene versus controls, respectively. Legends highlight upregulated (red) or downregulated (blue) transcripts, as well as genes not passing cutoff criteria for FC (black) and FDR (gray). Selected representative genes are shown (n = 2 biological replicates per genotype). **F**. Distribution of diffusion pseudotime values of myHSC and lyHSC from aged WT mice (n = 642 cells across 2 biological replicates and 4 technical replicates). In the inner box plots of the violinplots, the white point shows median value, box limits indicate upper and lower quartiles, whiskers extend to minimum and maximum values. P values are shown. Statistical significance was assessed by two-tailed t-test (*P < 0.05, **P < 0.01), except for the diffusion pseudotime analysis where two-tailed Wilcoxon rank sum test was used. Mean +/- SEM are shown.

https://doi.org/10.1038/s43587-024-00798-7

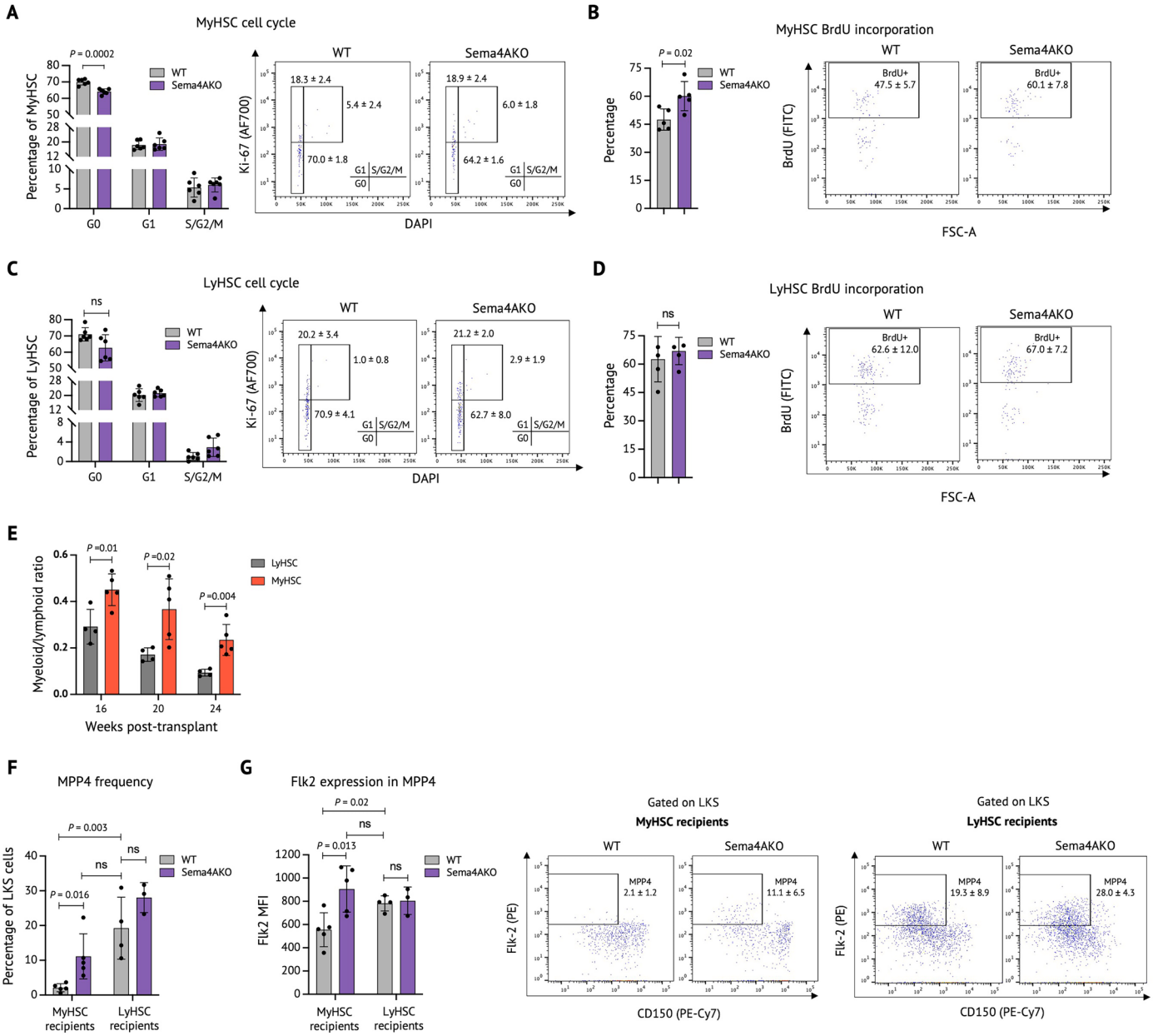

Extended Data Fig. 3 | The absence of Sema4A in young animals leads to selective myHSC hyperactivation at the steady state. A, B. MyHSC cell cycle analysis (n = 6 mice per group) **(A)** and myHSC short-term (4-day) BrdU incorporation (n = 5 mice per group) **(B)** in WT/Sema4AKO mice. **C, D.** LyHSC cell cycle analysis (n = 6 mice per group) **(C)** and lyHSC short-term (4-day) BrdU incorporation (n = 4 mice per group) **(D)** in WT/Sema4AKO mice. **E.** Myeloid/lymphoid ratio of peripheral blood donor-derived cells in WT mice (CD45.1) which were competitively transplanted with WT myHSC or LyHSC (CD45.2). **F, G.** Frequency **(F)** and mean fluorescent intensity of Flk2 expression **(G)** of MPP4 in the bone marrow of WT mice (CD45.1) after competitive transplantation of WT/Sema4AKO myHSC (myHSC recipients) (CD45.2) and WT/Sema4AKO lyHSC (lyHSC recipients) (CD45.2). Quantification and representative plots are shown (n = 5 for myHSC recipient groups, n = 4 for WT lyHSC recipient group and n = 3 for Sema4AKO lyHSC recipient group). P values are shown. Statistical significance was assessed by two-tailed t-test. Mean +/- SEM are shown.

https://doi.org/10.1038/s43587-024-00798-7

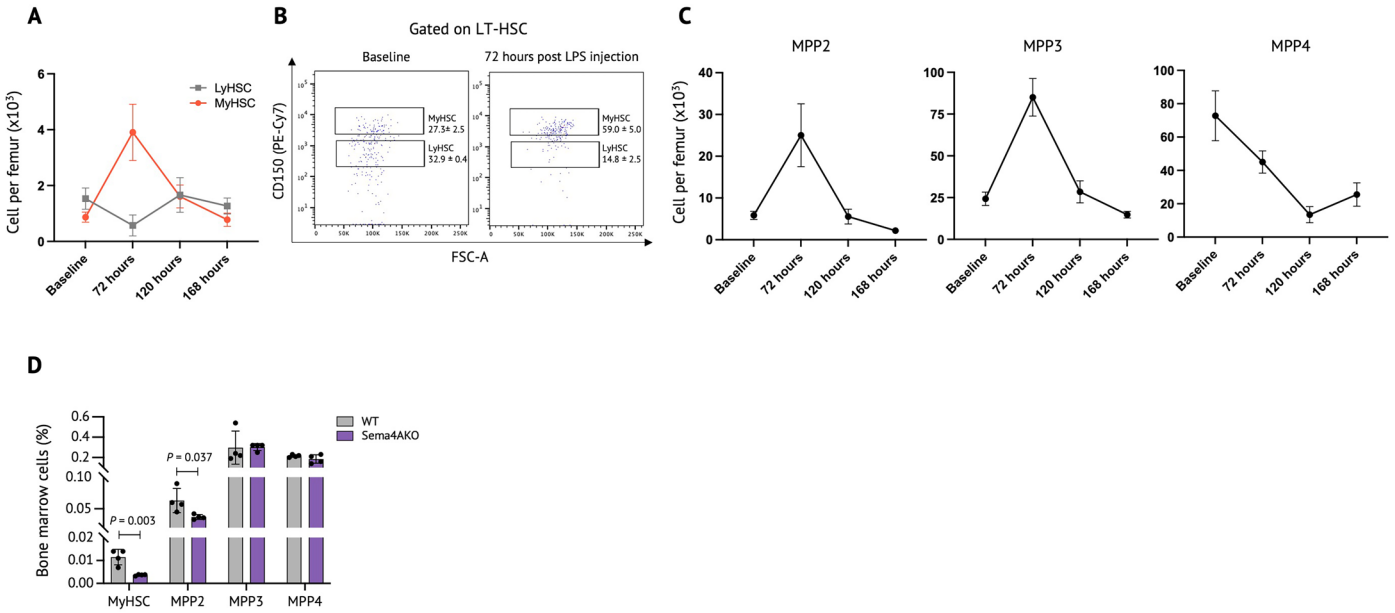

Extended Data Fig. 4 | Sema4AKO myHSC are hypersensitive to acute innate immune activation. A. Absolute number of WT myHSC/lyHSC at baseline and post-LPS injection at indicated time points (n = 5 mice for baseline group, n = 6 mice for 72 hours group, n = 7 mice for 120 hours group, n = 4 mice for 168 hours group). **B.** Representative flow cytometry plots of myHSC at baseline and 72 hours after LPS injection. **C.** Absolute number of WT MPPs at baseline and post-LPS injection at indicated time points (n = 5 mice for baseline group, n = 6 mice for 72 hours group, n = 7 mice for 120 hours group, n = 4 mice for 168 hours group). **D.** Frequency of myHSC and MPPs in WT/Sema4AKO mice 72 hours post-LPS injection (n = 4 mice per group). P values are shown. *P < 0.05, **P < 0.01. Statistical significance was assessed by two-tailed *t*-test. Mean +/- SEM are shown.

https://doi.org/10.1038/s43587-024-00798-7

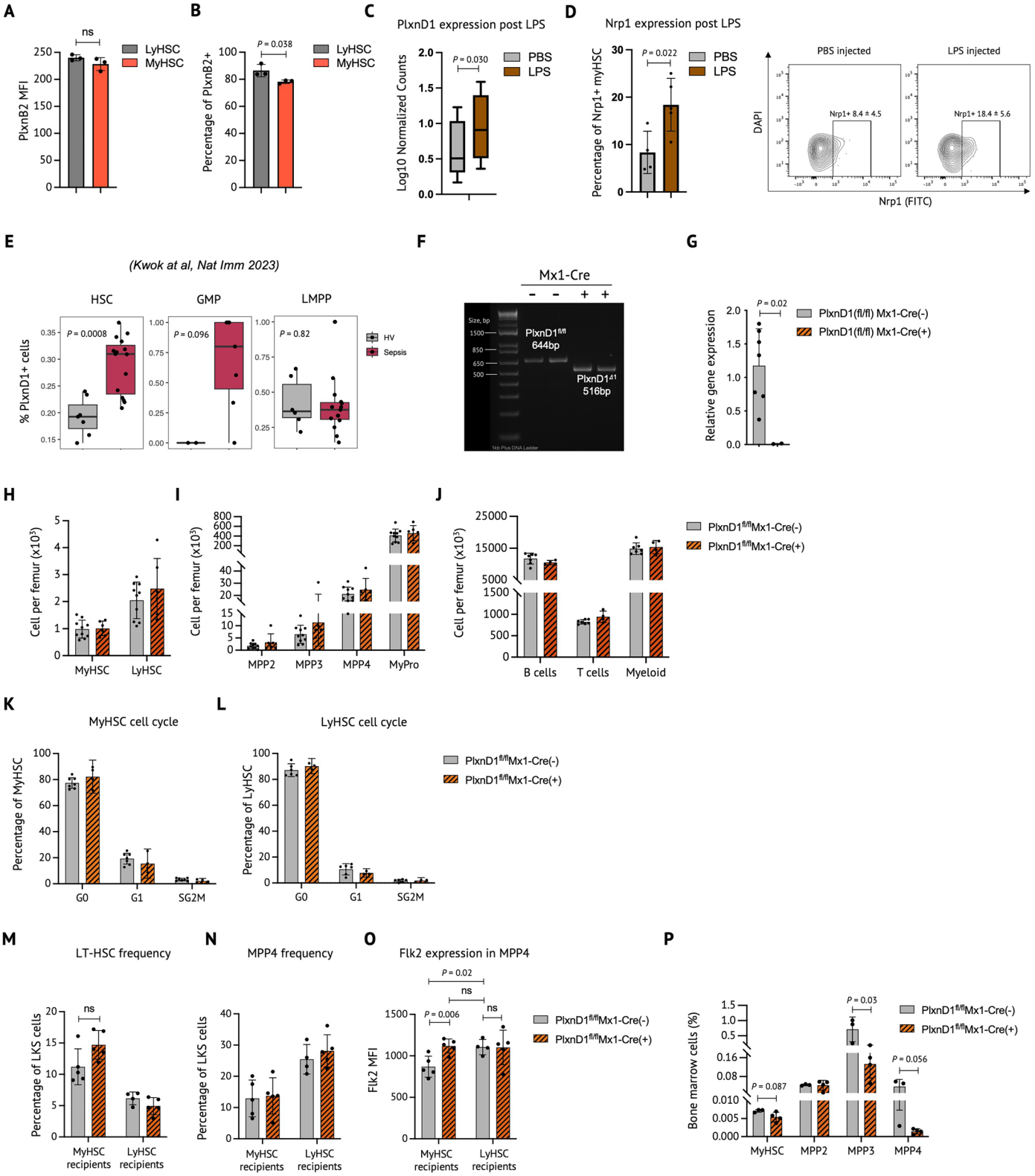

Extended Data Fig. 5 | See next page for caption.

https://doi.org/10.1038/s43587-024-00798-7

Extended Data Fig. 5 | PlxnD1$^{fl/fl}$ is a functional receptor for Sema4A on myHSC. **A**. Expression of PlxnB2 in myHSC and lyHSC in WT mice (n = 3 mice per group). **B**. Frequency of PlxnB2-expressing myHSC and lyHSC in WT mice (n = 3 mice per group). **C, D**. Expression of PlxnD1 mRNA in WT myHSC (n = 4 mice per group) **(C)** and percentage of Nrp1-expressing WT myHSC **(D)** 72 hours post-LPS injection, as assessed by RNA-Seq and flow cytometry, respectively (n = 4 mice for PBS group and n = 5 mice for LPS group). **E**. Frequency of PlxnD1^{+} CD34^{+} hematopoietic stem/progenitor cells in patients with sepsis, as assessed by scRNA Seq in Kwok et al[61]. Displayed is a cumulative analysis of "non-zero" PlxnD1 expression values in single HSPC obtained from 26 patients with sepsis and 6 healthy volunteers. **F, G**. PlxnD1 excision validation in Lin^{-}Kit^{+}Sca1^{+} cells by genomic DNA PCR (n = 2 mice per group) **(F)** and Q-PCR (n = 7 mice for PlxnD1fl/fl Cre(-) group and n = 3 mice for PlxnD1fl/fl Cre(+) group) **(G)**. **H-L**. Absolute number of myHSC and lyHSC (n = 10 mice for PlxnD1fl/fl Cre(-) group and n = 6 mice for PlxnD1fl/fl Cre(+) group) **(H)**, other primitive hematopoietic cells (n = 10 mice for PlxnD1fl/fl Cre(-) group and n = 6 mice for PlxnD1fl/fl Cre(+) group) **(I)**, mature cells (n = 7 mice for PlxnD1fl/fl Cre(-) group and n = 4 mice for PlxnD1fl/fl Cre(+) group) **(J)**, myHSC cell cycle analysis (n = 7 mice for PlxnD1fl/fl Cre(-) group and n = 4 mice for PlxnD1fl/fl Cre(+) group) **(K)**, lyHSC cell cycle analysis (n = 7 mice for PlxnD1fl/fl Cre(-) group and n = 4 mice for PlxnD1fl/fl Cre(+) group) **(L)** in PlxnD1fl/fl Mx1Cre(+) and PlxnD1fl/fl Cre(-) mice at baseline (n = 5 mice for PlxnD1fl/fl Cre(-) group and n = 3 mice for PlxnD1fl/fl Cre(+) group). **M**. Frequency of LT-HSC in the bone marrow of WT mice (CD45.1) after competitive transplantation of PlxnD1fl/fl Mx1Cre(+) and PlxnD1fl/fl Cre(-) myHSC (myHSC recipients) (CD45.2) and PlxnD1fl/fl Mx1Cre(+) and PlxnD1fl/fl Cre(-) lyHSC (lyHSC recipients) (CD45.2) (n = 5 mice for myHSC receipient groups, n = 4 mice for PlxnD1fl/fl Cre(-) lyHSC recipient group and n = 5 mice for PlxnD1fl/fl Cre(+) lyHSC recipient group). **N, O**. Frequency **(N)** and mean fluorescent intensity of Flk2 expression **(O)** of MPP4 in the bone marrow of WT mice (CD45.1) after competitive transplantation of PlxnD1fl/fl Mx1Cre(+) and PlxnD1fl/fl Cre(-) myHSC (myHSC recipients) and PlxnD1fl/fl Mx1Cre(+) and PlxnD1fl/fl Cre(-) lyHSC (lyHSC recipients), quantification and representative plots are shown for MPP4 frequency (n = 5 mice for myHSC receipient groups, n = 4 mice for PlxnD1fl/fl Cre(-) lyHSC recipient group and n = 5 mice for PlxnD1fl/fl Cre(+) lyHSC recipient group). **P**. Frequency of myHSC and MPPs in PlxnD1fl/fl Mx1Cre(+) and PlxnD1fl/fl Cre(-) mice 72 hours post-LPS injection (n = 3 mice for PlxnD1fl/fl Cre(-) group and n = 4 mice for PlxnD1fl/fl Cre(+) group). P values are shown. Statistical significance was assessed by two-tailed *t*-test. Mean +/- SEM are shown.

https://doi.org/10.1038/s43587-024-00798-7

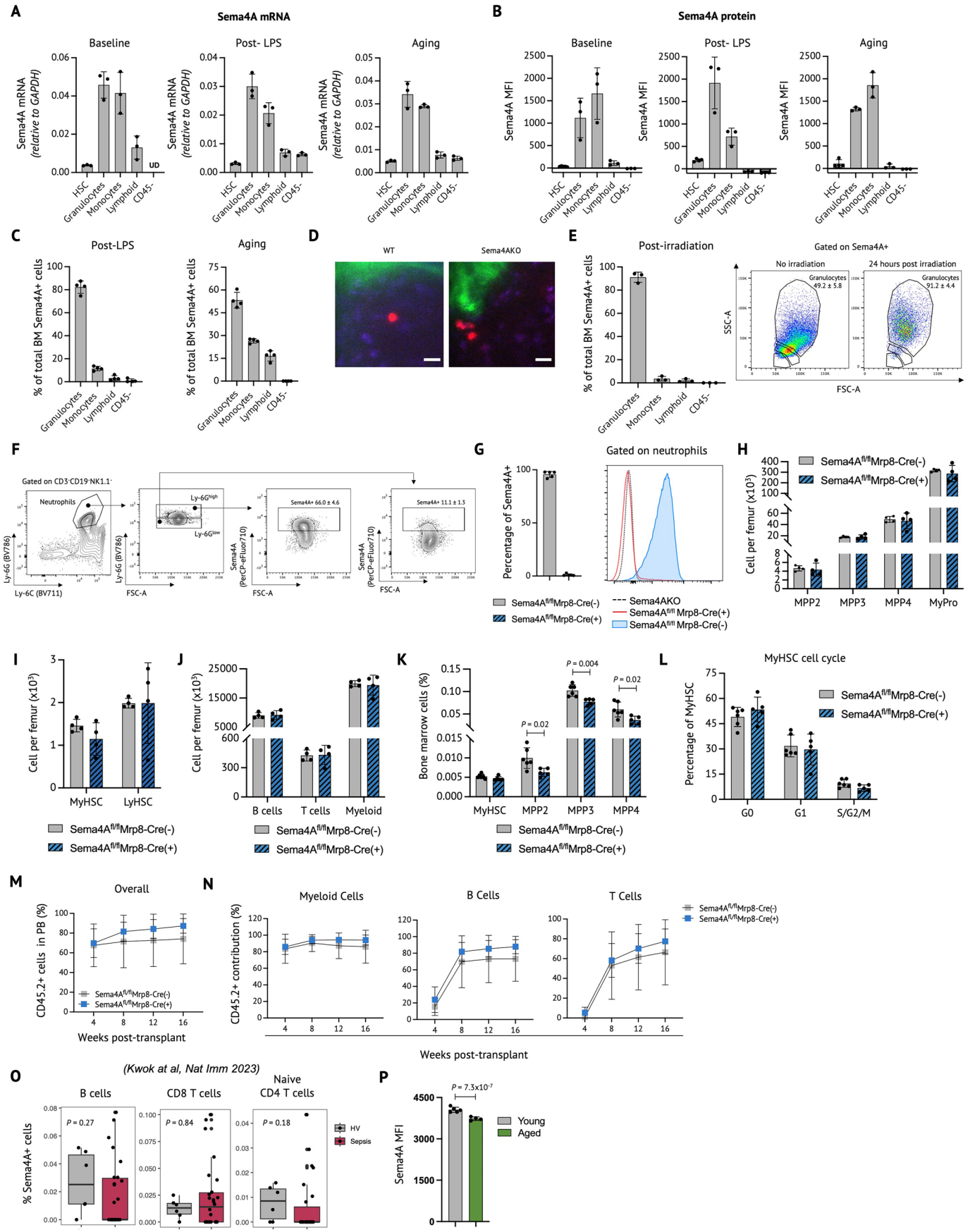

Extended Data Fig. 6 | See next page for caption.

https://doi.org/10.1038/s43587-024-00798-7

Extended Data Fig. 6 | Neutrophils serve as a physiologically important source of Sema4A. A, B. Sema4A mRNA **(A)** and protein expression **(B)** at baseline, 24 hours after LPS injection and upon aging (n = 3 mice per group per condition). **C**. Relative contribution of distinct cellular subsets to Sema4A production in the bone marrow 24 hours after LPS injection and upon aging (n = 4 mice per group)**. D**. Representative calviarial intra-vital microscopy images of WT myHSC transplanted into lethally irradiated WT/Sema4AKO recipients. Red – progeny of transplanted myHSC, green – bone, blue – collagen. Scale bar – 10 microne. **E**. Relative contribution of distinct cellular subsets to Sema4A production in the bone marrow 24 hours after 950 cGy irradiation, as estimated by flow cytometry with Sema4A antibody (n = 3 mice per group). Bar graph and representative flow cytometry plots are shown. **F**. Gating strategy for assessing Sema4A expression in $Ly6G^{high}$ vs $Ly6G^{low}$ neutrophils. **G**. Quantification and representative histogram of Sema4A deletion from neutrophils in $Sema4A^{fl/fl}$ Mrp8-Cre(+) mice (n = 5 mice per group). Sema4A antibody-stained neutrophils from Sema4AKO mouse were used as a negative control. **H-J**. Absolute number of primitive hematopoietic cells **(H)**, myHSC and lyHSC **(I)** and mature cells **(J)** at baseline in $Sema4A^{fl/fl}$ Mrp8-Cre(+) and $Sema4A^{fl/fl}$ Mrp8-Cre(-) mice (n = 4 mice per group). **K**. Frequency of myHSC and MPPs in $Sema4A^{fl/fl}$ Mrp8-Cre(+) and $Sema4A^{fl/fl}$ Mrp8-Cre(-) mice 72 hours after LPS injection (n = 6 mice for $Sema4A^{fl/fl}$ Mrp8-Cre(-) group and n = 5 mice for $Sema4A^{fl/fl}$ Mrp8-Cre(+) group). **L**. Cell cycle analysis of myHSC from $Sema4A^{fl/fl}$ Mrp8-Cre(+) and $Sema4A^{fl/fl}$ Mrp8-Cre(-) mice 72 hours after LPS injection (n = 6 mice for $Sema4A^{fl/fl}$ Mrp8-Cre(-) group and n = 5 mice for $Sema4A^{fl/fl}$ Mrp8-Cre(+) group). **M, N**. Overall percentage of donor-derived peripheral blood cells **(M)** and lineage contribution by donor-derived cells **(N)** in WT mice (CD45.1) which were competitively transplanted with myHSC from low-dose LPS-treated $Sema4A^{fl/fl}$ Mrp8-Cre(+) and $Sema4A^{fl/fl}$ Mrp8-Cre(-) (CD45.2) mice (n = 5 mice per group). **O**. Frequency of $Sema4A^{+}$ cells in peripheral blood lymphoid subsets from patients with sepsis and healthy volunteers (HV), as assessed by single cell RNA-Seq in Kwok et al.[61]. Displayed is a cumulative analysis of "non-zero" PlxnD1 expression values in single HSPC obtained from 26 patients with sepsis and 6 healthy volunteers. The plots show the median (middle line), interquartile range (box) and minimum to maximum values (whiskers) throughout. **P**. Sema4A mean fluorescent intensity of $Sema4A^{+}Ly6G^{high}$ neutrophils in the bone marrow of young and aged WT mice (n = 5 mice for young WT group and n = 4 mice for aged WT group). P values are shown. Statistical significance was assessed by two-tailed *t*-test. Mean +/- SEM are shown.

nature portfolio

Corresponding author(s): Lev Silberstein

Last updated by author(s): Dec 2, 2024

Reporting Summary

Nature Portfolio wishes to improve the reproducibility of the work that we publish. This form provides structure for consistency and transparency in reporting. For further information on Nature Portfolio policies, see our Editorial Policies and the Editorial Policy Checklist.

Statistics

For all statistical analyses, confirm that the following items are present in the figure legend, table legend, main text, or Methods section.

n/a	Confirmed
☐	☒ The exact sample size (*n*) for each experimental group/condition, given as a discrete number and unit of measurement
☐	☒ A statement on whether measurements were taken from distinct samples or whether the same sample was measured repeatedly
☐	☒ The statistical test(s) used AND whether they are one- or two-sided *Only common tests should be described solely by name; describe more complex techniques in the Methods section.*
☒	☐ A description of all covariates tested
☐	☒ A description of any assumptions or corrections, such as tests of normality and adjustment for multiple comparisons
☐	☒ A full description of the statistical parameters including central tendency (e.g. means) or other basic estimates (e.g. regression coefficient) AND variation (e.g. standard deviation) or associated estimates of uncertainty (e.g. confidence intervals)
☐	☒ For null hypothesis testing, the test statistic (e.g. *F*, *t*, *r*) with confidence intervals, effect sizes, degrees of freedom and *P* value noted *Give P values as exact values whenever suitable.*
☒	☐ For Bayesian analysis, information on the choice of priors and Markov chain Monte Carlo settings
☒	☐ For hierarchical and complex designs, identification of the appropriate level for tests and full reporting of outcomes
☒	☐ Estimates of effect sizes (e.g. Cohen's *d*, Pearson's *r*), indicating how they were calculated

Our web collection on statistics for biologists contains articles on many of the points above.

Software and code

Policy information about availability of computer code

Data collection	The following machines were used for data collection FACS- LSR Fortessa (BD), FACSymphony A5 (BD), FACSAria II (BD), FACSymphony S6 (BD) RNA seq data- NovaSeq SP (Illumina) Complete blood count and cellularity data- Element HT5 (Heska)
Data analysis	GraphPad Prism 10, Excel (Version 16.88), FlowJo (10.9), DESeq2, R, Ensembl, GSEApy, STAR, GRCm39, MSugDB, GSEA, Cell Ranger (v3), Scanpy, Scrublet, UMAP, Leiden Clustering, Scarlet, Cutadapt, BWA aligner, MACS peak align, HOMER.

For manuscripts utilizing custom algorithms or software that are central to the research but not yet described in published literature, software must be made available to editors and reviewers. We strongly encourage code deposition in a community repository (e.g. GitHub). See the Nature Portfolio guidelines for submitting code & software for further information.

Data

Policy information about availability of data

All manuscripts must include a data availability statement. This statement should provide the following information, where applicable:

- Accession codes, unique identifiers, or web links for publicly available datasets
- A description of any restrictions on data availability
- For clinical datasets or third party data, please ensure that the statement adheres to our policy

All data were analyzed with standard programs and packages, as detailed in Methods. RNA-sequencing data from this study are available from ArrayExpress, E-MTAB-11359 (single cell RNA-Seq of aged WT/Sema4AKO myHSC and lyHSC) and E-MTAB-12890 (bulk RNA-Seq of WT/Sema4AKO myHSC/lyHSC at baseline and after acute LPS). ATAC-Seq data from this study is available from Gene Expression Omnibus, GSE281145. The GRCm39 mouse genome assembly dataset can be accessed through the following link https://www.ncbi.nlm.nih.gov/datasets/genome/GCF_000001635.27/ .

Research involving human participants, their data, or biological material

Policy information about studies with human participants or human data. See also policy information about sex, gender (identity/presentation), and sexual orientation and race, ethnicity and racism.

Reporting on sex and gender	NA
Reporting on race, ethnicity, or other socially relevant groupings	NA
Population characteristics	NA
Recruitment	NA
Ethics oversight	NA

Note that full information on the approval of the study protocol must also be provided in the manuscript.

Field-specific reporting

Please select the one below that is the best fit for your research. If you are not sure, read the appropriate sections before making your selection.

☒ Life sciences ☐ Behavioural & social sciences ☐ Ecological, evolutionary & environmental sciences

For a reference copy of the document with all sections, see nature.com/documents/nr-reporting-summary-flat.pdf

Life sciences study design

All studies must disclose on these points even when the disclosure is negative.

Sample size	No statistical method was used to determine sample size. The number of mice chosen for each experiment is based on the principal that minimal number of mice is used to have statistical power and is comparable to published literature for the same assays performed (Silberstein, Cell Stem Cell 2016)
Data exclusions	Data points were excluded if they were identified as outliers by the Grubb's test.
Replication	Bulk RNA sequencing, scRNA sequencing and transplant experiments were not replicated, but the biological replicates are included in the study. Other results are representative of successfully repeated experiments. Number of biological replicates is described in the figures.
Randomization	No randomization method was used to allocate mice to experimental groups. The mice from the different groups were mixed together to exclude cage effects as a covariate.
Blinding	Since the observer bias is not relevant for the majority of the in vivo experiments, no blinding was used during data collection. However, in the experiments involving image analysis (histology, intravital imaging), where the observer bias may have been a concern, the investigators were blinded to the genetic background of the animals.

Reporting for specific materials, systems and methods

We require information from authors about some types of materials, experimental systems and methods used in many studies. Here, indicate whether each material, system or method listed is relevant to your study. If you are not sure if a list item applies to your research, read the appropriate section before selecting a response.

Materials & experimental systems

n/a	Involved in the study
☐	☒ Antibodies
☒	☐ Eukaryotic cell lines
☒	☐ Palaeontology and archaeology
☐	☒ Animals and other organisms
☒	☐ Clinical data
☒	☐ Dual use research of concern
☒	☐ Plants

Methods

n/a	Involved in the study
☒	☐ ChIP-seq
☐	☒ Flow cytometry
☒	☐ MRI-based neuroimaging

Antibodies

Antibodies used

Biotin anti-mouse CD8a BD Biosciences Cat# 553029; RRID: AB_394567
Biotin anti-mouse CD3ε BD Biosciences Cat# 553060; RRID: AB_394593
Biotin anti-mouse B220 BD Biosciences Cat# 553086; RRID: AB_394616
Biotin anti-mouse CD4 BD Biosciences Cat# 553728; RRID: AB_395012
Biotin anti-CD11b BD Biosciences Cat# 553309; RRID: AB_394773
Biotin anti-mouse TER-119 BD Biosciences Cat# 553672; RRID: AB_394985
Biotin anti-mouse Ly-6G and Ly-6C (Gr-1) BD Biosciences Cat# 553125; RRID: AB_394641
AF700 anti-mouse CD11b (Mac1) Invitrogen Cat# 56-0112-82; RRID: AB_65758
BV570 anti-mouse Gr-1 BioLegend Cat# 108431; RRID: AB_10896783
BV785 anti-mouse/human B220 BioLegend Cat# 103245; RRID: AB_11218795
FITC anti-mouse B220 BD Biosciences Cat# 553087; RRID: AB_394617
APC anti-mouse CD3ε BioLegend Cat# 100312; RRID: AB_312677
FITC anti-mouse CD45.2 BioLegend Cat# 109806; RRID: AB_313443
BV421 anti-mouse CD45.1 BioLegend Cat# 110732; RRID: AB_2562563
PE-CF594 anti-mouse Ly-6A/E (Sca-1) BD Biosciences Cat# 562730; RRID: AB_2737751
BUV395 anti-mouse Ly-6A/E (Sca-1) BD Biosciences Cat# 566216; RRID: AB_2739606
APC anti-mouse CD117 (c-Kit) BD Biosciences Cat# 553356; RRID: AB_398536
PE anti-mouse CD117 (c-Kit) BD Biosciences Cat# 561075; RRID: AB_10563204
PerCP-Cy 5.5 mouse Lineage antibody cocktail BD Biosciences Cat# 561317; RRID: AB_10612020
APC-Cy7 anti-mouse CD48 BD Biosciences Cat# 561242; RRID: AB_10644381
PE/Cyanine7 anti-mouse CD150 (SLAM) BioLegend Cat# 115914; RRID: AB_439797
FITC anti-mouse CD34 BD Biosciences Cat# 553733; RRID: AB_395017
AF700 anti-mouse CD34 BD Biosciences Cat# 560518; RRID: AB_1727471
BV421 anti-mouse CD135 (Flk-2) BD Biosciences Cat# 566292; RRID: AB_2739665
PE anti-mouse CD135 (Flk-2) BD Biosciences Cat# 553842; RRID: AB_395079
APC-Cy7 anti-mouse CD16/CD32 BD Biosciences Cat# 560541
BV510 anti-mouse CD41 BD Biosciences Cat# 740136; RRID: AB_2739892
BV786 anti-mouse CD105 BD Biosciences Cat# 564746; RRID: AB_2732065
FITC anti-mouse CD127 BioLegend Cat# 135007; RRID: AB_1937231
AF700 mouse anti-Ki-67 BD Biosciences Cat# 561277; RRID: AB_10611571
PE anti-mouse CD11c BioLegend Cat# 117307; RRID: AB_313776
BV605 anti-mouse CD11b BioLegend Cat# 101257; RRID: AB_2565431
BV711 anti-mouse Ly-6C BioLegend Cat# 128037; RRID: AB_2562630
AF647 anti-mouse Siglec-F BD Biosciences Cat# 562680 ; RRID: AB_2687570
PE/Cyanine7 anti-mouse CD24 BioLegend Cat# 101822 ; RRID: AB_756048
BV785 anti-mouse Ly-6G BioLegend Cat# 127645 ; RRID: AB_2566317
AF700 anti-mouse I-A/I-E BioLegend Cat# 107622 ; RRID: AB_493727
APC/Fire™ 750 anti-mouse CD3ε BioLegend Cat# 100362 ; RRID: AB_2629687
APC/Fire™ 750 anti-mouse CD19 BioLegend Cat# 115558 ; RRID: AB_2572120
APC/Fire™ 750 anti-mouse NK-1.1 BioLegend Cat# 108752 ; RRID: AB_2629764
FITC anti-mouse CD45 BioLegend Cat# 103108; RRID: AB_312973
AF700 anti-mouse Plexin B2 R&D Systems Cat#; FAB6836N
PerCP-Cy 5.5 anti-mouse/human Sema4A Invitrogen Cat#; 46-975-341 RRID: AB_2573898

Validation

All the antibodies are from commercially available sources and have been validated and reported in publications.

Animals and other research organisms

Policy information about studies involving animals; ARRIVE guidelines recommended for reporting animal research, and Sex and Gender in Research

Laboratory animals

Wild-type C57Bl/6J, B6SJL, Mx1-Cre and Mrp8-Cre mice were obtained from Jackson laboratory. PlxnD1 conditional KO mice and PlxnD1-GFP were obtained from Dr Chenghua Gu, Harvard University. Sema4AKO mice were obtained from Dr. A Kumanogoh, University of Osaka. Sema4A conditional KO mice were obtained from Dr T Worzfeld, University of Marburg. Young mice ranged from 8-12 weeks old and aged mice ranged from 74-80 weeks old. All mice were housed on a 12–12 h light–dark cycle at 25 °C. Mice

	were provided with standard chow (PicoLab Rodent Diet 20, cat. no. 5053, LabDiet) and water ad libitum. Humidity was kept at 30–70%. On-site veterinarians provided health status checks.
Wild animals	This study did not involve wild animals.
Reporting on sex	Female mice were used for aging experiments and male mice were used for inflammation experiments. For all other experiments, both female and male mice were used.
Field-collected samples	This study did mot involve samples collected from the field.
Ethics oversight	All animal experiments were approved by the Institutional Animal Care and Use Committee at Fred -Hutchinson Cancer Center

Note that full information on the approval of the study protocol must also be provided in the manuscript.

Plants

Seed stocks	NA
Novel plant genotypes	NA
Authentication	NA

Flow Cytometry

Plots

Confirm that:

☒ The axis labels state the marker and fluorochrome used (e.g. CD4-FITC).

☒ The axis scales are clearly visible. Include numbers along axes only for bottom left plot of group (a 'group' is an analysis of identical markers).

☒ All plots are contour plots with outliers or pseudocolor plots.

☒ A numerical value for number of cells or percentage (with statistics) is provided.

Methodology

Sample preparation	Whole bone-marrow mononuclear cells (BMMNC) were collected by crushing tibias, femurs, and pelvis in Ca2+/Mg2+-free phosphate-buffered saline (D-PBS) supplemented with 2% fetal bovine serum (FBS, Fisher Scientific). Cells were stained with antibodies for 30-90 minutes. Samples were washed with D-PBS+2% FBS before flow cytometry analysis. For cell sorting, BMMNC were lineage depleted by staining with CD3ε, CD11b, B220, TER-119, Gr-1, CD4 and CD8α biotin-conjugated antibodies (all from BD Biosciences) followed by application of streptavidin microbeads (Miltenyi Biotec) and depletion using magnetic separation columns (Miltenyi Biotec). DAPI was added to cells just prior to flow cytometry analysis.
Instrument	LSR Fortessa (BD), FACSymphony A5 (BD), FACSAria II (BD), FACSymphony S6 (BD)
Software	Data was collected with BD FACSDiva software and analyzed with FlowJo (Tree Star)
Cell population abundance	myHSC and lyHSC are very rare populations, around 0.001-0.004% of bone marrow cells
Gating strategy	We first used FSC-A/SSC-A to gate non-debris and then FSC-A/FSC-H and SSC-A/SSC-H to gate singlets. Single color controls were used to set up positive populations and FMO controls and, where possible, biological negative controls, were used to set negative populations. The detailed downstream gating strategies are included in the Figures.

☒ Tick this box to confirm that a figure exemplifying the gating strategy is provided in the Supplementary Information.